

# Benchmark of $GW$ Methods for Core-Level Binding Energies

Jiachen Li,<sup>†</sup> Ye Jin,<sup>†</sup> Patrick Rinke,<sup>‡</sup> Weitao Yang,<sup>†</sup> and Dorothea Golze<sup>\*,¶,‡</sup>

<sup>†</sup>*Department of Chemistry, Duke University, Durham, NC 27708, USA*

<sup>‡</sup>*Department of Applied Physics, Aalto University, Otakaari 1, FI-02150 Espoo, Finland*

<sup>¶</sup>*Faculty of Chemistry and Food Chemistry, Technische Universität Dresden, 01062 Dresden, Germany*

E-mail: dorothea.golze@tu-dresden.de

## Abstract

The  $GW$  approximation has recently gained increasing attention as a viable method for the computation of deep core-level binding energies as measured by X-ray photoelectron spectroscopy (XPS). We present a comprehensive benchmark study of different  $GW$  methodologies (starting-point optimized, partial and full eigenvalue-self-consistent, Hedin shift and renormalized singles) for molecular inner-shell excitations. We demonstrate that all methods yield a unique solution and apply them to the CORE65 benchmark set and ethyl trifluoroacetate. Three  $GW$  schemes clearly outperform the other methods for absolute core-level energies with a mean absolute error of 0.3 eV with respect to experiment. These are partial eigenvalue self-consistency, in which the eigenvalues are only updated in the Green's function, single-shot  $GW$  calculations based on an optimized hybrid functional starting point and a Hedin shift in the Green's function. While all methods reproduce the experimental relative binding energies well, the eigenvalue self-consistent schemes and the Hedin shift yield with mean errors  $< 0.2$  eV the best results.

# 1 INTRODUCTION

X-ray photoelectron spectroscopy (XPS) is a standard characterization tool for materials,<sup>1</sup> liquids<sup>2,3</sup> and molecules.<sup>4</sup> In XPS, the core-level binding energies (CLBEs) are measured,<sup>5</sup> which are element-specific, but also sensitive to the chemical environment. However, establishing the link between the measured spectrum and the atomic structure is challenging, in particular for complex materials with heavily convoluted XPS signals.<sup>6,7</sup> Guidance from theory is thus often necessary to interpret XPS spectra.

Theoretical XPS methods can be distinguished into Delta and response approaches. In Delta-based methods, the CLBE is computed as the total energy difference between the neutral and core-excited system. These calculations can be performed at different levels of theory, for example, with high-level wave-function methods, such as Delta coupled cluster ( $\Delta$ CC)<sup>8,9</sup> or with Kohn-Sham density functional theory<sup>10-12</sup> (KS-DFT). The most popular DFT-based approach is the Delta self-consistent field ( $\Delta$ SCF) method,<sup>13</sup> which has been thoroughly benchmarked.<sup>14-19</sup> While high accuracy can be achieved with these approaches, the explicit optimization of a core-ionized wave function leads to conceptual problems, e.g., regarding periodicity, constraining spin-orbit coupled states or, in the case of DFT, deteriorating accuracy for larger structures, which was already discussed and demonstrated elsewhere.<sup>20-24</sup>

An explicit orbital optimization of core-ionized systems and the related conceptual issues are avoided in response theories, where electron propagators are applied to transform the ground into an excited state. Recently, wave-function-based methods, such as linear response and equation-of-motion CC methods<sup>25-28</sup> and the algebraic diagrammatic construction method<sup>27</sup> were reassessed for absolute CLBEs, yielding partly promising results. Another promising approach in the realm of response methods is the *GW* approximation<sup>29-31</sup> to many-body perturbation theory, which is derived from Hedin's equation<sup>32</sup> by omitting the vertex correction. The *GW* approximation is considered the "gold standard" for the computa-

tion of band structures of materials,<sup>30,33</sup> but it has also been successfully applied to valence excitations of molecules.<sup>30,34–36</sup>

Due to its primary application to solids, *GW* was traditionally implemented in plane wave codes that typically use pseudo potentials for the deeper states. With the increasing availability of the *GW* method in localized basis set codes,<sup>37–44</sup> core states moved into focus. Core-level binding energy calculations have emerged as a recent trend in *GW*.<sup>21,23,43–51</sup> By extension to the Bethe-Salpeter equation (BSE@*GW*) also *K*-edge transition energies measured in X-ray absorption spectroscopy can be calculated.<sup>52</sup> These studies focused primarily on molecules. However, *GW* is one of the most promising methods for core-level predictions of materials because the scaling with respect to system size is generally smaller than for wave-function based response methods and the method is well-established for periodic structures. In addition, *GW* implementations for localized basis sets are advancing rapidly. Recently, periodic implementations<sup>43,53,54</sup> and low-scaling *GW* algorithms with  $O(N^3)$  complexity emerged in localized basis sets formulations.<sup>42,55–58</sup>

The application of *GW* to core states is more difficult than for valence states. We showed that more accurate and computationally more expensive techniques for the frequency integration of the self-energy are required compared to valence excitations.<sup>21</sup> Furthermore, we found that the standard single-shot  $G_0W_0$  approach performed on top of DFT calculations with generalized gradient approximations (GGAs) or standard hybrid functionals fails to yield a distinct solution, which is caused by a loss of spectral weight in the quasiparticle (QP) peak.<sup>48</sup> We demonstrated that eigenvalue self-consistency in  $G$  or using a hybrid functional with 45% exact exchange as starting point for the  $G_0W_0$  calculation restores the QP main excitation. Including also relativistic corrections,<sup>49</sup> an agreement of 0.3 eV and 0.2 eV with respect to experiment was reported for absolute and relative CLBEs, respectively.<sup>48</sup>

While  $G_0W_0$  is the computationally least expensive *GW* flavor, it strongly depends on the density functional approximation (DFA). Tuning the exchange in the hybrid functional to, e.g., 45% is conceptually unappealing and introduces undesired small species dependencies,

as discussed more in detail in this work. Self-consistency reduces or removes the dependence on the underlying DFT functional, but significantly increases the computational cost. The computationally least expensive self-consistent schemes are the so-called eigenvalue self-consistent approaches, where the eigenvalues are iterated in the Green’s function  $G$  (ev $GW_0$ ) or alternatively in  $G$  and the screened Coulomb interaction  $W$  (ev $GW$ ).<sup>30</sup> Higher-level self-consistency schemes, such as fully-self-consistent  $GW$ <sup>59–61</sup> (sc $GW$ ) and quasiparticle self-consistent  $GW$ <sup>62</sup> (qs $GW$ ) remove, unlike ev $GW_0$  or ev $GW$ , the starting point dependence completely. However, these higher-level self-consistency schemes are much more expensive and not necessarily better because of the inherent underscreening due to the missing vertex correction.<sup>63,64</sup>

Recently, we proposed the renormalized singles (RS) Green’s function approach, denoted as  $G_{\text{RS}}W_0$ , to reduce the starting point dependence in  $GW$ .<sup>65</sup> The RS concept was developed in the context of the random phase approximation (RPA) for accurate correlation energies,<sup>66,67</sup> and termed renormalized single-excitation (RSE) correction. Following standard perturbation theory, single-excitations contribute to the second-order correlation energy. It was shown that their inclusion significantly improves binding energies.<sup>66,67</sup> The RS Green’s function approach extends the RSE idea from correlation energies to  $GW$  QP energies. In the  $G_{\text{RS}}W_0$  scheme, the RS Green’s function is used as a new starting point and the screened Coulomb interaction is calculated with the KS Green’s function. For valence excitations, we found that this renormalization process significantly reduces the starting point dependence and provides improved accuracy over  $G_0W_0$ .<sup>65</sup> The mean absolute errors obtained from the  $G_{\text{RS}}W_0$  approach with different DFAs are smaller than 0.2 eV for predicting ionization potentials of molecules in the  $GW100$  set.<sup>65</sup> Unlike the self-consistent schemes, the RS Green’s function method hardly increases the computational cost compared to  $G_0W_0$ .

Recently, we employed the concept of RS in a multireference DFT approach for strongly correlated systems.<sup>68</sup> We also used the RS Green’s function in the T-matrix approximation ( $G_{\text{RS}}T_{\text{RS}}$ ) in a similar manner as in  $G_{\text{RS}}W_{\text{RS}}$ .<sup>69</sup> The T-matrix method scales formally as  $\mathcal{O}(N^6)$

with respect to system size  $N$ ,<sup>69,70</sup> with reduced scaling possible using effective truncation of the active space.<sup>71</sup> In addition to the high computational cost, the performance of  $G_{\text{RS}}T_{\text{RS}}$  for core-levels is not particularly impressive. The error with respect to experiment is 1.5 eV for absolute and 0.3 eV for relative CLBEs.<sup>69</sup> In the present work, we focus thus on RS  $GW$  approaches for core-levels.

In this work, we benchmark  $GW$  approaches, which we consider computationally affordable and suitable for large-scale applications. This includes  $G_0W_0$  with tuned starting points, the eigenvalue self-consistent schemes  $\text{ev}G_0W_0$  and  $\text{ev}GW$  and two new methods that we introduce in this work. One is based on the so-called Hedin shift<sup>72</sup> and can be understood as approximation of the  $\text{ev}G_0W_0$  method. We refer to this scheme as  $G_{\Delta\text{H}}W_0$ . The other is a different flavor of the RS Green’s function approach, where the screened Coulomb interaction is also computed with the RS Green’s function ( $G_{\text{RS}}W_{\text{RS}}$ ).

The remainder of this article is organized as follows: We introduce the different  $GW$  approaches in Section 2 and give the computational details for our calculations in Section 3. The solution behavior of the different methods is discussed in Section 4.1 by comparing self-energy matrix elements and spectral functions. In Section 4.2 results are presented for the CORE65 benchmark set and in Section 4.3 for the ethyl trifluoroacetate molecule and we finally draw conclusions in Section 5.

## 2 THEORY

### 2.1 Single-shot $G_0W_0$ approach

The most popular  $GW$  approach is the single-shot  $G_0W_0$  scheme, where the  $GW$  QP energies are obtained as corrections to the KS eigenvalues  $\{\epsilon_n^0\}$ :

$$\epsilon_n^{\text{QP}} = \epsilon_n^0 + \text{Re} \langle \psi_n^0 | \Sigma(\epsilon_n^{\text{QP}}) - v^{\text{xc}} | \psi_n^0 \rangle. \quad (1)$$

$\{\psi_n^0\}$  are the KS molecular orbitals (MOs) and  $v^{xc}$  is the KS exchange-correlation potential. We use  $i, j$  for occupied orbitals and  $a, b$  for virtual orbitals, and  $m, n$  for general orbitals. We omitted the spin index in all equations for simplicity and use the notation  $\Sigma_n = \langle \psi_n^0 | \Sigma | \psi_n^0 \rangle$  and  $v_n^{xc} = \langle \psi_n^0 | v^{xc} | \psi_n^0 \rangle$  in the following. We can directly obtain the CLBE of state  $n$  from the QP energies because they are related by  $\text{CLBE}_n = -\epsilon_n^{\text{QP}}$ . The self-energy  $\Sigma$  is given by

$$\Sigma(\mathbf{r}, \mathbf{r}', \omega) = \frac{i}{2\pi} \int d\omega' G_0(\mathbf{r}, \mathbf{r}', \omega + \omega') W_0(\mathbf{r}, \mathbf{r}', \omega') e^{i\omega'\eta} \quad (2)$$

where the non-interacting KS Green's function is denoted  $G_0$  and the screened Coulomb interaction  $W_0$ .  $\eta$  is a positive infinitesimal. The KS Green's function reads

$$G_0(\mathbf{r}, \mathbf{r}', \omega) = \sum_m \frac{\psi_m^0(\mathbf{r}) \psi_m^0(\mathbf{r}')}{\omega - \epsilon_m^0 - i\eta \text{sgn}(\epsilon_F - \epsilon_m^0)} \quad (3)$$

where  $\epsilon_F$  is the Fermi energy. The screened Coulomb interaction is calculated at the level of the RPA as

$$W_0(\mathbf{r}, \mathbf{r}', \omega) = \int d\mathbf{r}'' \varepsilon^{-1}(\mathbf{r}, \mathbf{r}'', \omega) v(\mathbf{r}'', \mathbf{r}') \quad (4)$$

where  $\varepsilon(\mathbf{r}, \mathbf{r}', \omega)$  is the dielectric function and  $v(\mathbf{r}, \mathbf{r}') = 1/|\mathbf{r} - \mathbf{r}'|$  the bare Coulomb interaction.

The calculation of the self-energy matrix elements  $\Sigma_n$  is split into a correlation part  $\Sigma^c$  and an exchange part  $\Sigma^x$ , i.e.,  $\Sigma_n = \Sigma_n^c + \Sigma_n^x$ . The HF-like exchange part  $\Sigma_n^x$  is given by

$$\Sigma_n^x = - \sum_i^{\text{occ}} \langle \psi_n^0 \psi_i^0 | \psi_i^0 \psi_n^0 \rangle. \quad (5)$$

The correlation part  $\Sigma^c$  is computed from  $W_0^c = W_0 - v$  and is the part that we plot in Section 4.1 to investigate the  $GW$  solution behavior. The correlation part in its fully analytic form is given by

$$\Sigma_n^c(\omega) = \sum_m \sum_s \frac{|\langle \psi_n^0 \psi_m^0 | \rho_s^0 \rangle|^2}{\omega - \epsilon_m^0 + (\Omega_s^0 - i\eta) \text{sgn}(\epsilon_F - \epsilon_m^0)}, \quad (6)$$

where  $\Omega_s^0$  are charge neutral excitations at the RPA level and  $\rho_s^0$  are the corresponding transition densities. The fully analytic form of  $\Sigma_n^c$  directly shows the pole structure of the self-energy and is illustrative to understand the solution behavior of  $GW$ . However, the evaluation of  $\Omega_s^0$  scales with  $O(N^6)$ . In practice, the correlation self-energy is usually evaluated with a reduced scaling by using techniques such as analytical continuation<sup>43,50</sup> or the contour deformation.<sup>21,43,73</sup>

The QP energies can be obtained by solving Equation (1), which is typically the computationally least expensive approach. In this work, we additionally employ two alternative approaches to obtain further insight into the physics and suitability of the different  $GW$  approaches. The first is the graphical solution of Equation (1), where we plot the self-energy matrix elements  $\Sigma_n^c$  and determine the QP solution by finding the intersections with the straight line  $\omega - \epsilon_n^0 + v_n^{\text{xc}} - \Sigma_n^x$ . The presence of several intersections would indicate that more than one solution exists. The second, computationally even more expensive alternative, is the computation of the spectral function,<sup>48</sup> which is given by

$$A(\omega) = \frac{1}{\pi} \sum_m \frac{|\text{Im}\Sigma_m(\omega)|}{[\omega - \epsilon_m - (\text{Re}\Sigma_m(\omega) - v_m^{\text{xc}})]^2 + [\text{Im}\Sigma_m(\omega)]^2} \quad (7)$$

In Equation (7), we include also the imaginary part of the complex self-energy, which gives us direct access to the spectral weights and satellite spectrum. At the  $G_0W_0$  level, we only use the diagonal elements of  $\Sigma$  in Equation (7).

## 2.2 Eigenvalue-selfconsistent $GW$ schemes

Including self-consistency in Hedin's  $GW$  equations is a widely used strategy to go beyond  $G_0W_0$ .  $\text{sc}GW$ <sup>30,61</sup> is conceptually the purest approach, but also the most expensive one. To reduce the computational demands, different lower-level self-consistent schemes were developed. The simplest approach is an eigenvalue self-consistent scheme, which comes in two different flavors. The first one is to iterate the eigenvalues only in  $G$  and keep  $W$  fixed

at the  $W_0$  level. This scheme is referred to as the  $evGW_0$  approach. In  $evGW_0$ , we start by updating the KS eigenvalues in the Green's function with the  $G_0W_0$  QP energies, re-evaluate the QP equation (see Equation (1)) and iterate until self-consistency in  $G$  is reached. The Green's function in the eigenvalue self-consistent scheme reads

$$G_{ev}(\mathbf{r}, \mathbf{r}', \omega) = \sum_m \frac{\psi_m^0(\mathbf{r})\psi_m^0(\mathbf{r}')}{\omega - \epsilon_m^{QP} - i\eta \text{sgn}(\epsilon_F - \epsilon_m^{QP})} \quad (8)$$

with  $\epsilon_m^{QP} = \epsilon_m^0 + \Delta\epsilon_m$ , where  $\Delta\epsilon_m$  is the  $GW$  correction, see Equation (1). The second flavor is  $evGW$ , where the KS eigenvalues are not only updated in  $G$ , but also in the screened Coulomb interaction  $W$ . The eigenvalue self-consistent calculations are computationally significantly more expensive than a  $G_0W_0$  calculation, in particular in combination with the accurate self-energy integration techniques that are required for core-levels.<sup>21</sup> The computational demands are large because  $G$ , the screened Coulomb interaction  $W$  (in the case of  $evGW$ ) and the self-energy have to be built repeatedly. In addition, Equation (1) must be solved not only for the states of interest, but for all states.

### 2.3 $GW$ with Hedin shift

The cost of an  $evGW_0$  scheme can be drastically reduced by using a global shift  $\Delta H$  instead of an individual shift  $\Delta\epsilon_m$  for each state  $m$ . This scheme was first introduced by Hedin<sup>32</sup> and is referred to as  $G_{\Delta H}W_0$  in the following. The  $G_{\Delta H}W_0$  approach was discussed several times in the literature<sup>29,72,74,75</sup> and the effect of  $evGW_0$  and the  $G_{\Delta H}W_0$  on the self-energy structure has been discussed for valence states in Ref. 30. In the Hedin-shift scheme, the Green's function transforms into

$$G_{\Delta H}(\mathbf{r}, \mathbf{r}', \omega) = \sum_m \frac{\psi_m^0(\mathbf{r})\psi_m^0(\mathbf{r}')}{\omega - (\epsilon_m^0 + \Delta H) - i\eta \text{sgn}(\epsilon_F - \epsilon_m^0)}, \quad (9)$$



where  $G_0(\omega - \Delta H) = G_{\Delta H}(\omega)$ . The QP equation with the Hedin-shift scheme then becomes

$$\epsilon_n^{\text{QP}} = \epsilon_n^0 + \text{Re} \langle \psi_n^0 | \Sigma(\epsilon_n^{\text{QP}} - \Delta H) - v^{\text{xc}} | \psi_n^0 \rangle. \quad (10)$$

Traditionally,  $\Delta H$  is determined with respect to the Fermi level of  $G_0$  for metals or the valence band maximum for gapped solid-state systems. For the molecular case,  $\Delta H$  is evaluated with respect to the highest occupied molecular orbital (HOMO) by introducing the self-consistency condition  $\epsilon_{\text{HOMO}}^{\text{QP}} = \epsilon_{\text{HOMO}}^0 + \Delta H$ , which is inserted in Equation (10) and yields

$$\Delta H_{\text{HOMO}} = \text{Re} \Sigma_{\text{HOMO}}(\epsilon_{\text{HOMO}}^0) - v_{\text{HOMO}}^{\text{xc}}. \quad (11)$$

As demonstrated in Ref. 30,  $\text{ev}GW_0$  and the  $G_{\Delta H}W_0$  lead to a shift of the pole structure of the self-energy matrix elements  $\Sigma_n$  to more negative frequencies. For  $\Sigma_{\text{HOMO}}(\omega)$ , the shift is similar for  $\text{ev}GW_0$  and  $G_{\Delta H}W_0$  yielding practically the same  $\epsilon_{\text{HOMO}}^{\text{QP}}$ .

For core states, we found that the shift  $\Delta H$  computed as in Equation (11) is much smaller than the one from  $\text{ev}GW_0$ . We propose here a new approach, where we calculate the shift  $\Delta H$  for the core state of interest as

$$\Delta H_{\text{core}} = \text{Re} \Sigma_{\text{core}}(\epsilon_{\text{core}}^0) - v_{\text{core}}^{\text{xc}}. \quad (12)$$

For example, to obtain  $\epsilon_{\text{C1s}}^{\text{QP}}$  for the CO molecule, we solve Equation (10) with  $\Delta H_{\text{C1s}}$ , whereas we solve it with  $\Delta H_{\text{O1s}}$  for  $\epsilon_{\text{O1s}}^{\text{QP}}$ . In the case of HCOOH, we determine  $\Delta H_{\text{core}}$  for each O separately.

In a  $G_{\Delta H}W_0$  calculation, we calculate  $\Delta H$  once, insert it in Equation (10) and iterate the latter as in a regular  $G_0W_0$  calculation. The shift  $\Delta H$  is kept constant during the iteration of the QP equation. Compared to a  $G_0W_0$  calculation, the computation of  $\Delta H$  is the only computational overhead that we introduced. The computational cost of a  $G_{\Delta H}W_0$  calculation

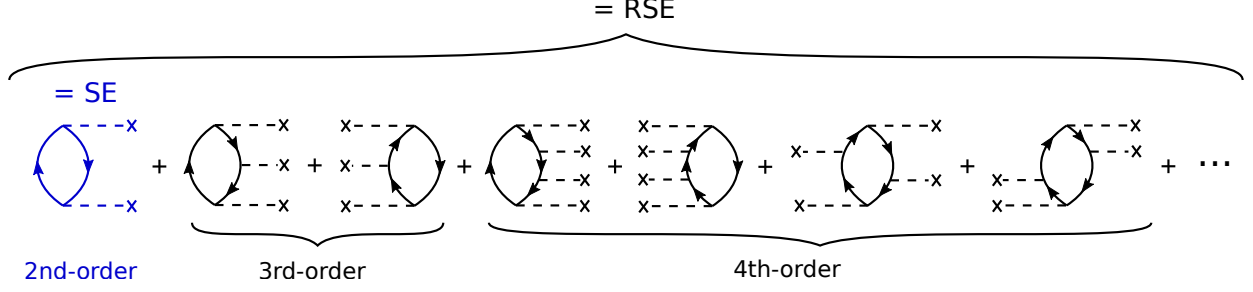


Figure 1: Goldstone diagrammatic for the renormalized singles contributions. Dashed lines, which end with a cross denote the matrix elements  $\langle \psi_p | v^{\text{HF}} - v^{\text{Hxc}} | \psi_q \rangle$

is thus practically the same as for a  $G_0W_0$  calculation. The  $G_{\Delta\text{H}}W_0$  method can be viewed as a one-diagonal element correction in the context of the  $\text{ev}GW_0$  method.

## 2.4 Renormalized singles excitations in RPA

The RS Green's function approach is based on the same idea as the RSE corrections in RPA. Since we consider the introduction of the RS concept more illustrative for total than QP energies, we will briefly summarize the key equations derived by Ren *et al.*<sup>66,67,76</sup> in the context of Rayleigh-Schrödinger perturbation theory (RSPT), before proceeding with the RS Green's function approaches in Section 2.5.

In RSPT, the interacting  $N$ -electron Hamiltonian  $\hat{H}$  is partitioned into a non-interacting mean-field Hamiltonian  $\hat{H}_0$  and an interacting perturbation  $\hat{H}'$ .

$$\hat{H}_0 = \sum_i^N \hat{h}^0(j) = \sum_{j=1}^N \left[ -\frac{1}{2} \nabla_j^2 + v_{\text{ext}}(\mathbf{r}_j) + v_j^{\text{Hxc}} \right] \quad (13)$$

$$\hat{H}' = \sum_{j < k}^N \frac{1}{|\mathbf{r}_j - \mathbf{r}_k|} - \sum_{j=1}^N v_j^{\text{Hxc}} \quad (14)$$

where  $\hat{h}_0$  is the single-particle Hamiltonian of the mean field reference. The Hamiltonian  $\hat{h}_0$  includes the kinetic term, the external potential  $v_{\text{ext}}$  and the mean-field potential  $v^{\text{Hxc}}$ . The latter can be the single-particle potential from HF or KS-DFT and contains the Hartree and exchange-correlation terms. Following standard perturbation theory, single-excitations (SE)

contribute to the second-order correlation energy and are given by<sup>66,67</sup>

$$E_c^{\text{SE}} = \sum_i^{\text{occ}} \sum_a^{\text{virt}} \frac{|\langle \Psi_0 | \hat{H}' | \Psi_i^a \rangle|^2}{\epsilon_i^0 - \epsilon_a^0} \quad (15)$$

$$= \sum_i^{\text{occ}} \sum_a^{\text{virt}} \frac{|\langle \psi_i^0 | v^{\text{HF}} - v^{\text{Hxc}} | \psi_a^0 \rangle|^2}{\epsilon_i^0 - \epsilon_a^0} \quad (16)$$

where  $|\Psi_0\rangle$  is the Slater determinant for the ground state configuration and  $|\Psi_i^a\rangle$  for the singly excited configuration. The orbitals  $\psi_{i/a}^0$  and corresponding orbital energies  $\epsilon_{i/a}^0$  are the ones of the  $\hat{h}^0(j)$  operator. The derivation of Equation (16) from Equation (15) is given in detail in the supporting information (SI) of Ref. 66. As evident from Equation (16), the singles correction vanishes if  $v^{\text{Hxc}}$  is the HF mean-field potential, which is a consequence of Brillouin's theorem.<sup>77</sup>

The energy  $E_c^{\text{SE}}$  is only the second-order correction to the correlation energy, as shown in Figure 1. The infinite summation of the higher-order diagrams yields the renormalized singles excitation (RSE) correction. The derivation of the RSE correlation energy is given in detail in Ref. 67. To summarize briefly the procedure, the Fock matrix is evaluated with the KS orbitals. Subsequently, the occupied and unoccupied blocks of this matrix are diagonalized separately (subspace diagonalization), which yields a new set of (RS) eigenvalues and orbitals. Replacing  $\psi_{i/a}$  and  $\epsilon_{i/a}$  in Equation 16 with the RS eigenvalues and orbitals yields the RSE correlation energy.

## 2.5 RS Green's function GW approaches

In analogy to the RPA RSE correction, the RS Green's function  $G_{\text{RS}}$  is designed as an effective non-interacting reference system that includes all the single contributions. The RS Green's function is defined as

$$G_{\text{RS}}^{-1} = G_0^{-1} - P(\Sigma_{\text{HF}}[G_0] - v^{\text{Hxc}})P - Q(\Sigma_{\text{HF}}[G_0] - v^{\text{Hxc}})Q, \quad (17)$$

where  $P = \sum_i^{\text{occ}} |\psi_i^0\rangle\langle\psi_i^0|$  is the projection into the occupied orbital space and  $Q = I - P$  is the projection into the virtual orbital space.  $\Sigma_{\text{HF}}[G_0]$  refers to a HF-like self-energy constructed with  $G_0$ , which is usually the KS Green's function.  $\Sigma_{\text{HF}}$  is the sum of the Hartree self-energy  $\Sigma^{\text{H}}$  and the exchange self-energy  $\Sigma^x$ , i.e.,  $\Sigma_{\text{HF}} = \Sigma^{\text{H}} + \Sigma^x$ , where  $\Sigma_{mn}^{\text{H}} = \sum_i^{\text{occ}} \langle\psi_m^0\psi_i^0 | \psi_n^0\psi_i^0\rangle$  and  $\Sigma_{mn}^x = -\sum_i \langle\psi_m^0\psi_i^0 | \psi_i^0\psi_n^0\rangle$ . Note that both are built with the mean-field orbitals  $\psi_n^0$  provided by, e.g., KS-DFT.  $v^{\text{Hxc}}$  is the single-particle Hartree-exchange-correlation potential defined in Equation (13). If the potential  $v^{\text{Hxc}}$  is the one from HF and if  $G_0$  is the HF Green's function, then the second and third term on the right-hand-side of Equation (17) vanish and  $G_{\text{RS}}$  corresponds to the HF Green's function, which is again a consequence of Brillouin's theorem.  $G_{\text{RS}}$  includes the singles contributions, which are one source of the starting point dependence. As we showed previously,<sup>65</sup> the dependence on the DFA is therefore reduced in the  $G_{\text{RS}}W_0$  scheme.

The RS Green's function is given as the solution of the two projected equations in the occupied orbital subspace<sup>65</sup>

$$P(G_{\text{RS}}^{-1})P = P(G_0^{-1})P + P(\Sigma_{\text{HF}}[G_0] - v^{\text{Hxc}})P, \quad (18)$$

and the virtual orbital subspace

$$Q(G_{\text{RS}}^{-1})Q = Q(G_0^{-1})Q + Q(\Sigma_{\text{HF}}[G_0] - v^{\text{Hxc}})Q. \quad (19)$$

In practice,  $G_{\text{RS}}$  is obtained by a similar subspace diagonalization procedure as used for the RSE total energy corrections. The KS density matrix is used to construct the HF Hamiltonian  $\hat{H}_{\text{HF}}$ , which defines the RS Hamiltonian  $\hat{H}_{\text{RS}} = \hat{H}_{\text{HF}}[G_0]$ . The equations for the occupied

$$P(\hat{H}_{\text{HF}}[G_0])P|\psi_i^{\text{RS}}\rangle = \epsilon_i^{\text{RS}}P|\psi_i^{\text{RS}}\rangle, \quad (20)$$

and virtual subspace

$$Q(\hat{H}_{\text{HF}}[G_0])Q|\psi_a^{\text{RS}}\rangle = \epsilon_a^{\text{RS}}Q|\psi_a^{\text{RS}}\rangle \quad (21)$$

are diagonalized separately.<sup>65</sup> The subspace diagonalization yields the RS eigenvalues  $\epsilon_n^{\text{RS}}$  and corresponding eigenvectors  $\psi_n^{\text{RS}}$  and is performed only once. The RS Green's function is computed with the RS eigenvalues and orbitals,

$$G_{\text{RS}}(\mathbf{r}, \mathbf{r}', \omega) = \sum_m \frac{\psi_m^{\text{RS}}(\mathbf{r})\psi_m^{\text{RS}}(\mathbf{r}')}{\omega - \epsilon_m^{\text{RS}} - i\eta\text{sgn}(\epsilon_F - \epsilon_m^{\text{RS}})}, \quad (22)$$

and is diagonal in the occupied subspace and the virtual subspace.

In the  $G_{\text{RS}}W_0$  approach,<sup>65</sup> the RS Green's function is used as a new starting point and the screened interaction is calculated with the KS Green's function. The correlation part of the  $G_{\text{RS}}W_0$  self-energy is<sup>65</sup>

$$\Sigma_n^{c, G_{\text{RS}}W_0}(\omega) = \sum_m \sum_s \frac{|\langle \psi_n^0 \psi_m^0 | \rho_s^0 \rangle|^2}{\omega - \epsilon_m^{\text{RS}} + (\Omega_s^0 - i\eta)\text{sgn}(\epsilon_m^{\text{RS}} - \epsilon_F)}, \quad (23)$$

where  $\rho_s^0$  and  $\Omega_s^0$  are the transition densities and the RPA excitation energies calculated with the KS Green's function. Then the QP equation for  $G_{\text{RS}}W_0$  is

$$\epsilon_n^{\text{QP}} = \epsilon_n^0 + \text{Re} \langle \psi_n^0 | \Sigma^{G_{\text{RS}}W_0}(\epsilon_n^{\text{QP}}) - v^{\text{xc}} | \psi_n^0 \rangle. \quad (24)$$

Note that Equations (23) and (24) are slightly different from the original QP equation for  $G_{\text{RS}}W_0$ ,<sup>65</sup> where we used the RS eigenvectors  $\psi_n^{\text{RS}}$ . Here we use for simplicity the KS instead of the RS orbitals because we found that the difference induced upon using RS orbitals is marginal.<sup>65</sup> Since we use the KS orbitals, the exchange part of the  $G_{\text{RS}}W_0$  self-energy is the same as in  $G_0W_0$ , see Equation (5).

In this work we introduce a new approach that uses the RS Green's function as a new starting point and also calculates the screened Coulomb interaction with the RS Green's function, denoted as  $G_{\text{RS}}W_{\text{RS}}$ . This means that  $W_{\text{RS}}$  is obtained by inserting the RS Green's

function into the RPA equation. Similar to  $G_{\text{RS}}W_0$ , the exchange part of the  $G_{\text{RS}}W_{\text{RS}}$  self-energy is also the same as  $G_0W_0$ , but the correlation part of the  $G_{\text{RS}}W_{\text{RS}}$  self-energy becomes

$$\Sigma_n^{c, G_{\text{RS}}W_{\text{RS}}}(\omega) = \sum_m \sum_s \frac{|\langle \psi_n^0 \psi_m^0 | \rho_s^{\text{RS}} \rangle|^2}{\omega - \epsilon_m^{\text{RS}} - (\Omega_s^{\text{RS}} - i\eta) \text{sgn}(\epsilon_m^{\text{RS}} - \epsilon_{\text{F}})}, \quad (25)$$

where  $\rho_s^{\text{RS}}$  and  $\Omega_s^{\text{RS}}$  are the transition densities and the RPA excitation energies calculated with the RS Green's function. Then the QP equation for the  $G_{\text{RS}}W_{\text{RS}}$  approach follows as

$$\epsilon_n^{\text{QP}} = \epsilon_n^0 + \text{Re} \langle \psi_n^0 | \Sigma^{G_{\text{RS}}W_{\text{RS}}}(\epsilon_n^{\text{QP}}) - v^{\text{xc}} | \psi_n^0 \rangle. \quad (26)$$

The construction of the RS Green's function scales only as  $\mathcal{O}(N^3)$  with respect to system size  $N$ . The overall scaling of  $G_{\text{RS}}W_{\text{RS}}$  depends on the frequency integration technique, which is  $\mathcal{O}(N^6)$  for a fully analytic evaluation of the self-energy using Equation (6), but  $\mathcal{O}(N^4)$  (valence states) or  $\mathcal{O}(N^5)$  (core states) with the contour deformation approach.<sup>21,43,73</sup> Given that the same frequency integration is used for  $G_0W_0$  and  $G_{\text{RS}}W_{\text{RS}}$ , the computational cost of a  $G_{\text{RS}}W_{\text{RS}}$  calculation is only marginally larger than for a  $G_0W_0$  calculation.

### 3 COMPUTATIONAL DETAILS

Core-level calculations were performed at the  $G_0W_0$ ,  $\text{ev}GW_0$ ,  $\text{ev}GW$ ,  $G_{\Delta\text{H}}W_0$  and  $G_{\text{RS}}W_{\text{RS}}$  level for the CORE65 benchmark set,<sup>48</sup> which contains 65 1s excitations energies of 32 small molecules ( $30 \times \text{C1s}$ ,  $21 \times \text{O1s}$ ,  $11 \times \text{N1s}$  and  $3 \times \text{F1s}$ ). Geometries and experimental reference values were taken from Ref. 48. Additionally, we studied the ethyl trifluoroacetate molecule. The structure of the latter was obtained upon request from the authors of Ref. 18 and is available in the SI.

The  $G_0W_0$ ,  $\text{ev}GW_0$ ,  $\text{ev}GW$  and  $G_{\Delta\text{H}}W_0$  calculations were carried out with the FHI-aims program package,<sup>78,79</sup> which is based on numeric, atom-centered orbitals (NAOs). The  $G_0W_0$  and  $\text{ev}GW_0$  data were extracted from our previous work,<sup>48</sup> while the  $\text{ev}GW$  and  $G_{\Delta\text{H}}W_0$

data were generated for this benchmark study. In the FHI-aims calculations, the contour deformation technique<sup>21,30,73</sup> is used to evaluate the self-energy, using a modified Gauss-Legendre grid<sup>38</sup> with 200 grid points for the imaginary frequency integral part. The  $G_{\text{RS}}W_{\text{RS}}$  calculations were performed with the QM4D program.<sup>80</sup> In QM4D, the  $GW$  self-energy integral is calculated fully analytically, see Equation (6). In FHI-aims and also in QM4D, the QP equation is always solved iteratively.

For  $\text{ev}GW_0$ ,  $\text{ev}GW$  and  $G_{\Delta\text{H}}W_0$ , we used the Perdew-Burke-Ernzerhof (PBE)<sup>81</sup> functional for the underlying DFT calculation, while the  $G_0W_0$  calculations employ the PBEh( $\alpha$ ) hybrid functional<sup>82</sup> with 45% exact exchange ( $\alpha = 0.45$ ). The  $G_{\text{RS}}W_{\text{RS}}$  calculations were performed with PBE and three different hybrid functionals, namely PBE0,<sup>83,84</sup> PBEh( $\alpha = 0.45$ ) and B3LYP.<sup>85,86</sup> Note that PBE0 corresponds to PBEh( $\alpha = 0.25$ ).

All  $GW$  results are extrapolated to the complete basis set limit using the Dunning basis set family  $\text{cc-pVnZ}$ .<sup>87,88</sup> Following Ref. 48, the extrapolation is performed by a linear regression with respect to the inverse of the total number of basis functions. A four-point extrapolation with  $n = 3 - 6$  is performed for  $G_0W_0$ ,  $\text{ev}GW_0$ ,  $\text{ev}GW$  and  $G_{\Delta\text{H}}W_0$ . For  $G_{\text{RS}}W_{\text{RS}}$ , we use only two points ( $n = 3, 4$ ) due to computational limitations. We verified that this two-point extrapolation deviates only by 0.1 eV from the four-point scheme on average. The  $\text{cc-pVnZ}$  family are contracted Gaussian-type orbitals (GTOs), which can be considered as a special case of an NAO and are treated numerically in FHI-aims. Note that the  $\text{cc-pVnZ}$  basis sets are treated as spherical GTOs in FHI-aims, whereas in QM4D they are processed as pure Cartesian GTOs. Both codes use the resolution-of-the-identity (RI) approach with the Coulomb metric (RI-V).<sup>89</sup> In FHI-aims, the RI auxiliary basis sets are generated on-the-fly as described in Ref. 38. For the QM4D calculations, the corresponding RI basis sets for  $\text{cc-pVTZ}$  and  $\text{cc-pVQZ}$  from Ref. 90 were used.

Relativistic effects were included for all calculations as post-processing step following the approach in Refs. 48 and 49, i.e., we performed a non-relativistic  $GW$  calculation on top of a non-relativistic KS-DFT calculation and added the corrective term derived in Ref. 49 to the

*GW* QP energies. The magnitude of the corrections increase with the atomic number and ranges from 0.12 eV for C1s to 0.71 eV for F1s. The relativistic corrections were derived for a free neutral atom at the PBE level and were obtained by evaluating the difference between the 1s eigenvalues from the radial KS and the 4-component Dirac-KS equation.

## 4 RESULTS AND DISCUSSIONS

### 4.1 Solution behavior

In our previous work<sup>48</sup> we showed that standard  $G_0W_0$  calculations starting from a GGA functional, which are routinely applied to valence states, lead to an erroneous multi-solution behavior for deep core states. It is thus important to confirm that the respective *GW* flavors yield indeed a unique solution. Only looking at the QP energies obtained by iterating Equation (1) is typically not enough to verify the latter. Detailed insight into the solution behavior of *GW*-based methods can be obtained by: i) plotting the real part of the correlation self-energy  $\Sigma^c$  and ii) plotting the spectral function  $A(\omega)$  as defined in Equation (7). In Figure 2, we investigate  $A(\omega)$  and the diagonal matrix elements  $\Sigma_n^c(\omega)$  for the 1s oxygen orbital of a single water molecule. Results are shown for  $G_0W_0$  and  $G_{\text{RS}}W_{\text{RS}}$  with different starting points (PBE, PBE0, B3LYP, PBEh( $\alpha = 0.45$ )) as well as partial self-consistent schemes, namely  $\text{ev}G_0W_0$ ,  $\text{ev}GW$  and  $G_{\Delta\text{H}}W_0$ , using PBE for the underlying DFT calculation.

We start our discussion with the  $G_0W_0$  spectral functions and self-energy elements displayed in Figure 2(a,b,d), where we reproduced for convenience the  $G_0W_0@$ PBE,  $G_0W_0@$ PBE0 and  $G_0W_0@$ PBEh( $\alpha = 0.45$ ) results, which were also presented in Ref. 48. Figure 2(b) shows the self-energy from a  $G_0W_0@$ PBE (gray line), which exhibits many poles. The poles are broadened by the  $\eta$ -term in Equation (3) and thus appear as spikes in the self-energy. For  $G_0W_0@$ PBE we find that the poles are located in the frequency region where the QP solution is expected (around 540 eV). As already outlined in Section 2.1, we can obtain the graphical solution of Equation (1) by finding the intersections with the straight line  $\omega - \varepsilon_n^0 + v_n^{xc} - \Sigma_n^x$ .



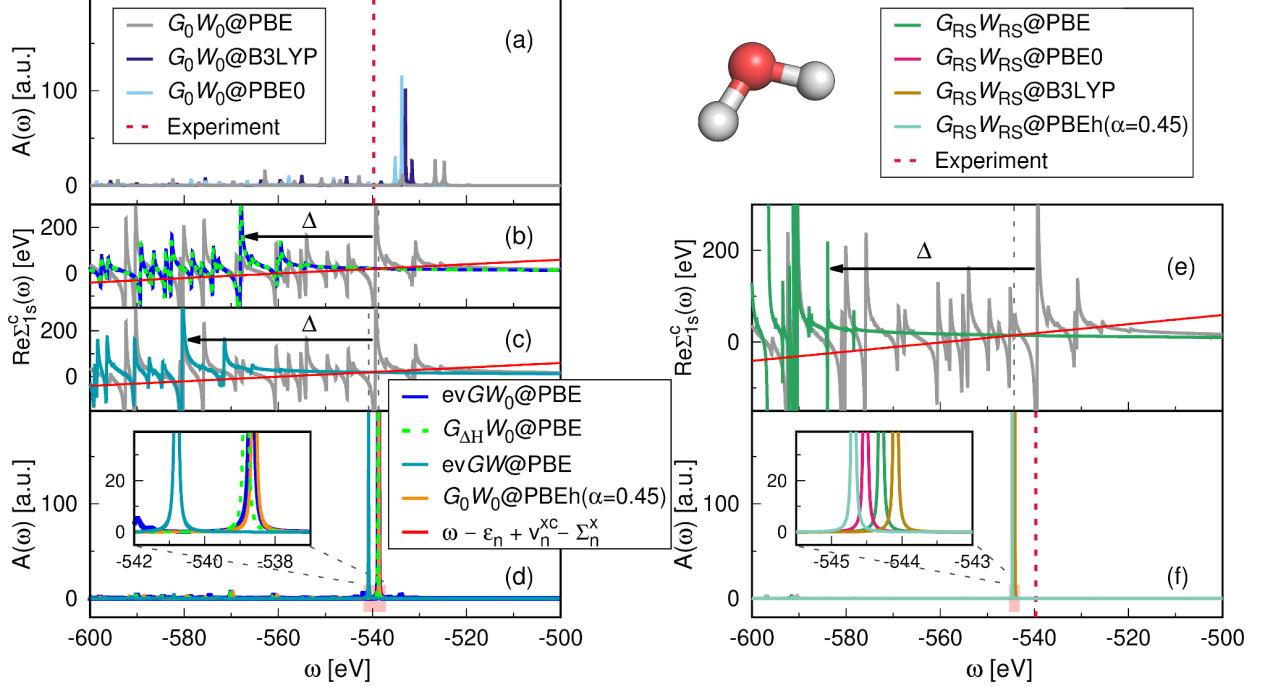


Figure 2: O1s excitation for a single water molecule from  $G_0W_0$ ,  $evGW_0$ ,  $G_{\Delta H}W_0$ ,  $evGW$  and  $G_{RS}W_{RS}$  computed at the cc-pVQZ level. (a) Spectral function  $A(\omega)$  (Equation (7)) from  $G_0W_0$  using starting points with no exact exchange or a low amount. (b,c) Real part of the correlation self-energy  $\Sigma^c(\omega)$  in  $evGW_0@PBE$ ,  $G_{\Delta H}W_0$  and  $evGW@PBE$ . Diagonal matrix elements  $\text{Re}\Sigma_n^c(\omega) = \langle \psi_n | \text{Re}\Sigma^c(\omega) | \psi_n \rangle$  for the oxygen 1s orbital. The intersection with the red line is the graphical solution of Equation (1). The vertical gray-dashed line indicates the QP solution of this graphical solution and  $\Delta$  indicates the shift with respect to  $G_0W_0@PBE$  (gray) (d) Spectral functions in  $evGW_0@PBE$ ,  $G_{\Delta H}W_0@PBE$ ,  $evGW@PBE$  and  $G_0W_0@PBEh(\alpha=0.45)$ . (e) Self-energy matrix elements  $\text{Re}\Sigma_n^c(\omega)$  in  $G_{RS}W_{RS}@PBE$  (green) compared to  $G_0W_0@PBE$  (gray). (f) Spectral functions  $A(\omega)$  in  $G_{RS}W_{RS}$  with different starting points.

For  $G_0W_0$ , we observe many intersections, which are all valid solutions of the QP equation. The corresponding spectral function in Figure 2(a) shows many peaks with equal spectral weight, but no clear main peak that could be assigned to the QP excitation in contrast to the experiment, where a sharp peak at 539.7 eV<sup>4</sup> is observed. A main peak starts to emerge for hybrid functional starting points, such as PBE0 ( $\alpha = 0.25$ ) and B3LYP ( $\alpha = 0.20$ ). However,  $G_0W_0@PBE0$  and  $G_0W_0@B3LYP$  still yield an unphysical second peak, which carries a large fraction of the spectral weight.

As already discussed in Ref. 48, the reason for this unphysical behavior is the overlap of the satellite spectrum with the QP peak. Satellites are due to multielectron excitations that accompany the photoemission process, e.g., shake-up satellites, which are produced when the core photoelectron scatters a valence shell electron to a higher unoccupied energy level.<sup>91,92</sup> These peaks appear as series of smaller peaks at higher energies than the QP energy. For molecules, the spectral weight of these peaks is orders of magnitudes smaller than for the main excitation.<sup>92</sup> Satellites occur in frequency regions where the real part of the self-energy has poles. As demonstrated in, e.g., Ref. 30, the imaginary part of the self-energy exhibits complementary peaks at these frequencies (Kramers-Kronig relation). According to Equation (7), large imaginary parts lead to peaks with small spectral weight, i.e., peaks with satellite character.

The occurrence of pole features around the QP excitations for deep core states can best be understood by analyzing the denominator of the fully analytic expression of the self-energy given in Equation (6).  $\Sigma_n^c(\omega)$  has poles on the real axis for  $\eta \rightarrow 0$  at  $\epsilon_i^0 - \Omega_s$  (occupied states  $i$ ) and  $\epsilon_a^0 + \Omega_s$  (virtual states  $a$ ). For occupied states, the eigenvalues  $\epsilon_i^0$  are too large (too positive) and the charge neutral excitations  $\Omega_s$  are underestimated at the PBE level. As a result, the poles  $\epsilon_i^0 - \Omega_s$  are at too positive frequencies and the satellite thus too close to the QP peak. For virtual states, the same reasoning holds for the poles  $\epsilon_a + \Omega_s$ , but with reversed sign, i.e., the poles are at too small frequencies. The separation between satellites and QP peak is also too small for valence excitations. However, the problem gets progressively worse further away from the Fermi level since the absolute differences between PBE eigenvalues  $\epsilon_i^0$  and the QP excitation increases. We demonstrated this for semi-core states,<sup>56</sup> for which a distinct QP peak is still obtained. However, for deep core states the separation becomes finally so small that the satellites merge with the QP peak.

The proper separation between QP excitation and satellites can be restored by using an  $evGW_0$  scheme. The  $evGW_0@PBE$  self-energy is shown in Figure 2(b) (reproduced from Ref. 48). Iterating the eigenvalues in  $G$  shifts the on-set of the pole structure too more

negative frequencies. The overall pole structure is very similar to  $G_0W_0@PBE$ , but shifted by a constant value of  $\Delta = -28.7$  eV. The  $G_{\Delta H}W_0@PBE$  self-energy displayed in Figure 2(b) is almost identical to  $evGW_0@PBE$ . The shift of the pole structure compared to  $G_0W_0@PBE$  is with  $\Delta = -28.8$  eV only slightly larger than for  $evGW_0$ . The rigid  $\Delta$ -shift of the poles features can be understood as follows: In  $evGW_0$  and  $G_{\Delta H}W_0$ , the KS eigenvalue  $\epsilon_m^0$  are replaced with  $\epsilon_m^0 + \epsilon_m$  and  $\epsilon_m^0 + \Delta H_{1s}$ , respectively, where  $\Delta\epsilon_m$  is the self-consistent  $GW$  correction for state  $m$  and  $\Delta H_{1s}$  its non-self-consistent approximation for the O1s state (see Equation (12)). The poles are consequently located at  $\epsilon_{1s} + \Delta\epsilon_{1s} - \Omega_s$  and  $\epsilon_{1s} + \Delta H_{1s} - \Omega_s$ . Since both corrections,  $\Delta\epsilon_{1s}$  and  $\Delta H_{1s}$  are negative for PBE starting points, the poles, i.e., satellites move to more negative frequencies and are properly separated from the main excitation. The spectral function now exhibits a distinct QP peak as evidenced by Figure 2(d).

As discussed in detail previously,<sup>48</sup> the effect of eigenvalue self-consistency can be mimicked in a  $G_0W_0$  calculation by using a hybrid functional with a high amount of exact exchange  $\alpha$ . We showed that increasing  $\alpha$  progressively shifts the pole features to more negative frequencies. For  $\alpha = 0.45$ , the  $evGW_0@PBE$  self-energy is approximately reproduced and the spectral function shows a distinct peak as displayed in Figure 2(d). We note here again that values of  $\alpha < 0.3$  do not yield a clear main peak<sup>48</sup> and thus no unique solution, which is also demonstrated in Figure 2(a).

The  $evGW$  approach and the  $G_{RS}W_{RS}$  schemes lead to a significantly stronger shift of the pole features than  $evGW_0@PBE$  or  $G_{\Delta H}W_0@PBE$ , as shown in Figure 2(c) and (e). The spectral functions displayed in Figure 2(d) and (f) confirm that  $evGW$  and the  $G_{RS}W_{RS}$  yield a distinct peak in the spectrum. The RS eigenvalues of the occupied orbitals are more negative and the ones of the virtual orbitals are more positive than the KS eigenvalues. In addition, RPA evaluated with RS fundamental gaps provides larger excitation energies  $\Omega_s$ . In  $G_{RS}W_{RS}$  the poles at  $\epsilon_a + \Omega_s$  are shifted in the positive direction and the poles at  $\epsilon_i - \Omega_s$  are shifted in the negative direction. Therefore, satellites from these poles are separated from the main peak. For  $G_{RS}W_{RS}$ , a unique solution is obtained for all starting points. As we show in

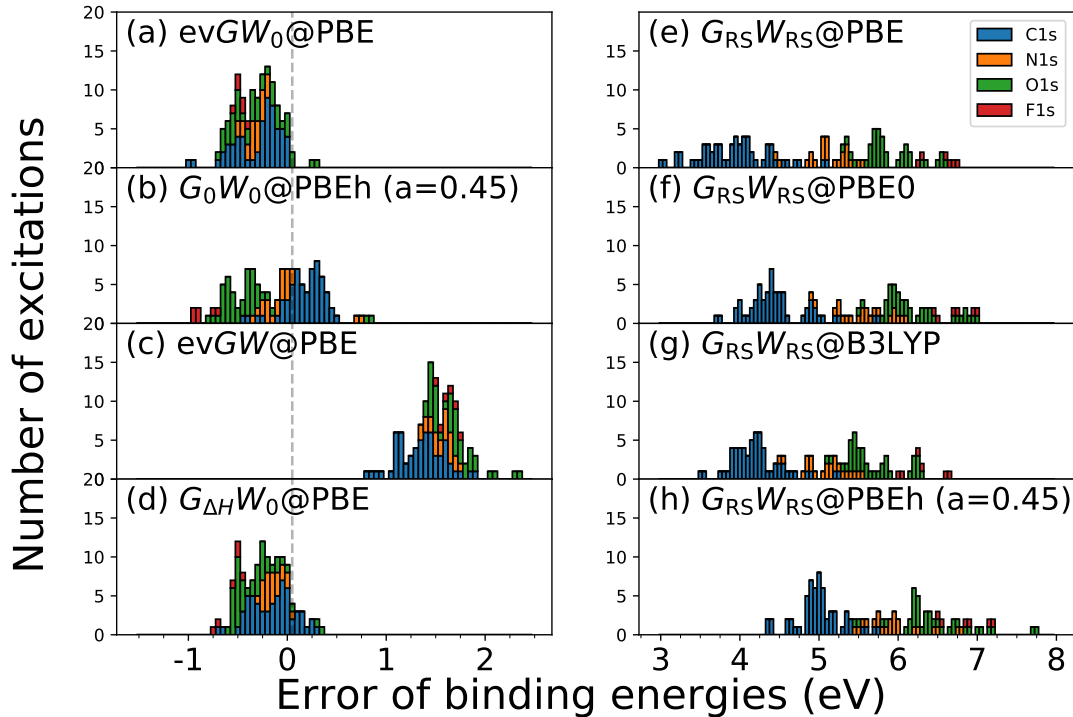


Figure 3: Distribution of errors with respect to the experiment for absolute 1s binding energies of the CORE65 benchmark set, where the error is defined as  $\text{Error}_i = \text{CLBE}_i^{\text{theory}} - \text{CLBE}_i^{\text{exp}}$ . The histogram is stacked. Eight  $GW$  approaches are compared: (a)  $\text{evGW}_0@PBE$ , (b)  $G_0W_0@PBEh$  ( $\alpha = 0.45$ ), (c)  $\text{evGW}@PBE$ , (d)  $G_{\Delta H}W_0@PBE$ , (e)  $G_{RS}W_{RS}@PBE$ , (f)  $G_{RS}W_{RS}@PBE0$ , (g)  $G_{RS}W_{RS}@B3LYP$ , (h)  $G_{RS}W_{RS}@PBEh$  ( $\alpha = 0.45$ ).

Figure S1 (see SI), the  $G_{RS}W_0$  approach suffers from a multi-solution behavior in the deep core region and cannot be applied for core-level calculations.

## 4.2 CORE65 benchmark

In the following, we discuss the CORE65 results for the  $GW$  schemes for which a physical solution behavior was confirmed in Section 4.1, namely  $\text{evGW}_0@PBE$ ,  $\text{evGW}@PBE$ ,  $G_0W_0@PBE(\alpha = 0.45)$ ,  $G_{\Delta H}W_0@PBE$  and  $G_{RS}W_{RS}$  with four different starting points (PBE, PBE0, B3LYP, PBEh( $\alpha = 0.45$ )). The distribution of the errors with respect to experiment are shown in Figure 3 and Figure 4 for the absolute CLBES and the relative CLBES, respectively. The corresponding mean absolute errors (MAE) and the mean errors (ME) are given in Table 1. The error of excitation  $i$  is defined as  $\text{Error}_i = \text{CLBE}_i^{\text{theory}} - \text{CLBE}_i^{\text{experiment}}$ .

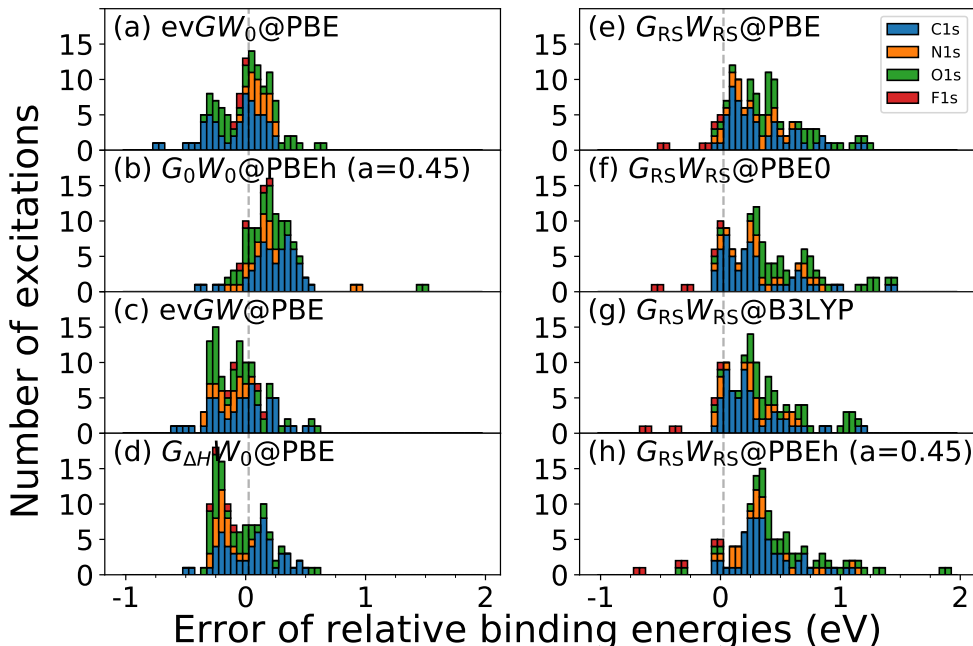


Figure 4: Distribution of errors with respect to the experiment for relative 1s binding energies of the CORE65 benchmark set. The histogram is stacked. CH<sub>4</sub>, NH<sub>3</sub>, H<sub>2</sub>O and CH<sub>3</sub>F have been used as reference molecules for C1s, N1s, O1s and F1s respectively. Eight GW approaches are compared: (a)  $evGW_0@PBE$ , (b)  $G_0W_0@PBEh(\alpha = 0.45)$ , (c)  $evGW@PBE$ , (d)  $G_{\Delta H}W_0@PBE$ , (e)  $G_{RS}W_{RS}@PBE$ , (f)  $G_{RS}W_{RS}@PBE0$ , (g)  $G_{RS}W_{RS}@B3LYP$ , (h)  $G_{RS}W_{RS}@PBEh(\alpha = 0.45)$ .

Starting the discussion with the absolute CLBEs, we find that  $evGW_0@PBE$ ,  $G_0W_0@PBEh(\alpha = 0.45)$  and  $G_{\Delta H}W_0@PBE$  yield the best results with error distributions close to zero and MAEs of  $\approx 0.3$  eV. The smallest overall MAE of 0.25 eV is obtained with  $G_{\Delta H}W_0@PBE$ . Figure 3(a) and (d) show that the errors from  $evGW_0@PBE$  and  $G_{\Delta H}W_0@PBE$  are tightly distributed, but mostly negative, i.e., the computed CLBEs are slightly underestimated. Generally, we find that the  $G_{\Delta H}W_0@PBE$  scheme reproduces the  $evGW_0@PBE$  results almost perfectly. The slight underestimation of the absolute CLBEs by  $evGW_0@PBE$  and  $G_{\Delta H}W_0@PBE$  might be due to insufficiencies in the  $cc\text{-}pVnZ$  basis sets, which are not captured by the extrapolation procedure. A very recent study<sup>51</sup> with  $G_0W_0@PBEh$  showed that increasing the number of core functions by, e.g., uncontracting the  $cc\text{-}pVnZ$  basis sets, yields larger absolute CLBEs. The reported increase is in the range of 0.25 to maximal

0.5 eV, indicating that the CLBES from  $evGW_0$  and  $G_{\Delta H}W_0@PBE$  might be even closer to experiment with core-rich basis sets.

The error distribution of  $G_0W_0@PBEh(\alpha = 0.45)$ , which is displayed in Figure 3(b), is centered around zero, yielding also the smallest overall ME, see Table 1. Compared to  $evGW_0@PBE$  and  $G_{\Delta H}W_0@PBE$ , the spread of the  $G_0W_0@PBEh$  errors is larger and a clustering by species can be observed. The C1s binding energies (BEs) are overestimated, while the N1s, O1s and F1s are increasingly underestimated. This is due to the species dependence of the  $\alpha$  parameter, which we discussed in Ref. 48. As we showed in Ref. 48, including relativistic effects reduces the species dependence of  $\alpha$ , but does not remove it completely. The optimal  $\alpha$  value,  $\alpha_{opt}$ , increases from 0.44 (C1s) to 0.49 (F1s), after including relativistic corrections. For  $\alpha < \alpha_{opt}$ , the CLBES are too small and for  $\alpha > \alpha_{opt}$  too large. As a result, the C1s BEs are overestimated for  $\alpha = 0.45$ , and O1s and F1s BEs are underestimated.

$evGW@PBE$  systematically overestimates the absolute CLBES by 1-2 eV since iterating also the eigenvalues in  $W$  effectively leads to an underscreening. At the PBE level, the fundamental gap is underestimated and inserting the PBE eigenvalues in  $W$  consequently yields an overscreened potential. However, the overscreening in  $W$  compensates the underscreening introduced by the missing vertex corrections. Comparing  $evGW_0@PBE$  and  $evGW@PBE$ , our observation for deep core-levels agrees with previous work, which found that  $evGW_0$  improves upon  $G_0W_0$ ,<sup>93,94</sup> while  $evGW$  yields too large band gaps<sup>93</sup> and overly stretched spectra.<sup>95</sup> Furthermore, the performance of  $evGW@PBE$  for deep core-levels seems to be comparable to higher-level self-consistency schemes such as  $qsGW$ .<sup>62</sup> An exploratory study by Setten *et al.*<sup>46</sup> reported that  $qsGW$  overestimates the absolute 1s BEs of small molecules by 2 eV. This indicates that  $qsGW$  suffers from similar underscreening effects and that the orbitals inserted in the  $GW$  scheme have a minor effect on core-level QP energies.

The error distributions for the absolute CLBES from  $G_{RS}W_{RS}$  are shown in Figure 3(e-h) for four different starting points.  $G_{RS}W_{RS}$  overestimates the absolute CLBES by 3-8 eV with

Table 1: Mean absolute error (MAE) and mean error (ME) in eV with respect to experiment for absolute and relative CLBEs of the CORE65 benchmark set. The error for excitation  $i$  is defined as  $\text{Error}_i = \text{CLBE}_i^{\text{theory}} - \text{CLBE}_i^{\text{exp}}$ . The relative CLBEs are the shifts with respect to a reference molecule,  $\Delta\text{CLBE} = \text{CLBE} - \text{CLBE}_{\text{ref\_mol}}$ . CH<sub>4</sub>, NH<sub>3</sub>, H<sub>2</sub>O and CH<sub>3</sub>F have been used as reference molecules for C1s, N1s, O1s and F1s respectively.

core-level	evGW <sub>0</sub> @		G <sub>0</sub> W <sub>0</sub> @		evGW@		G <sub>ΔH</sub> W <sub>0</sub> @		G <sub>RS</sub> W <sub>RS</sub> @							
	PBE		PBEh		PBE		PBE		PBE		PBE0		B3LYP		PBEh	
	MAE	ME	MAE	ME	MAE	ME	MAE	ME	MAE	ME	MAE	ME	MAE	ME	MAE	ME
Absolute CLBEs																
all	0.30	-0.29	0.33	-0.08	1.53	1.53	0.25	-0.20	4.88	4.88	5.32	5.32	4.94	4.94	5.72	5.72
C1s	0.27	-0.27	0.24	0.19	1.37	1.37	0.20	-0.13	3.97	3.97	4.50	4.50	4.24	4.24	5.03	5.03
N1s	0.30	-0.30	0.16	-0.01	1.58	1.58	0.14	-0.13	5.13	5.13	5.59	5.59	5.12	5.12	6.00	6.00
O1s	0.32	-0.28	0.48	-0.40	1.70	1.70	0.35	-0.31	5.91	5.91	6.24	6.24	5.71	5.71	7.48	7.48
F1s	0.44	-0.44	0.83	-0.83	1.65	1.65	0.54	-0.54	6.56	6.56	6.75	6.75	6.32	6.32	6.88	6.88
Relative CLBEs																
all	0.18	0.02	0.26	0.23	0.18	-0.03	0.19	-0.02	0.40	0.39	0.43	0.43	0.37	0.36	0.48	0.46
C1s	0.18	-0.05	0.29	0.25	0.19	-0.01	0.20	0.07	0.36	0.36	0.33	0.33	0.30	0.30	0.41	0.41
N1s	0.14	0.14	0.23	0.21	0.14	-0.13	0.16	-0.15	0.29	0.29	0.39	0.39	0.30	0.30	0.40	0.40
O1s	0.22	0.08	0.25	0.24	0.18	-0.03	0.20	-0.06	0.56	0.56	0.66	0.66	0.56	0.56	0.68	0.65
F1s	0.05	-0.05	0.11	0.10	0.11	0.02	0.16	-0.16	0.16	-0.10	0.16	0.00	0.20	0.02	0.22	0.00

an MAE between 5-6 eV. The reason for the large overestimation is that the RS fundamental gap is too large, which then leads, similarly as in  $G_0W_0@HF$ ,<sup>95</sup> to an underscreening in  $W$ . One way to reduce the underscreening is to include corrections for the electron correlation in the RS Hamiltonian, which is dominated by exchange interactions. An alternative strategy is to compensate the underscreening by including vertex corrections, e.g., to use the T-matrix formalism,<sup>29,69,70</sup> where the two-point screened interaction  $W$  is replaced with a four-point effective interaction  $T$ . However, methods such as the T-matrix are computationally much more expensive than  $GW$  due to their higher complexity. We recently applied the  $G_{RS}T_{RS}$  scheme to the CORE65 benchmark set.<sup>69</sup> Comparing  $G_{RS}W_{RS}$  and  $G_{RS}T_{RS}$ , the overestimation is indeed reduced by  $G_{RS}T_{RS}$ , which yields an ME of  $\approx 1.5$  eV. However, the errors for the absolute CLBEs are still an order of magnitude larger than for computationally cheaper schemes such as  $evGW_0$  or  $G_{\Delta H}W_0$ , which rely on a very fortunate error cancellation effect that leads to a balanced screening.

Furthermore, we find that the overestimation with  $G_{\text{RS}}W_{\text{RS}}$  increases with the atomic number, i.e., from the C1s to the F1s excitations. This species dependence is inherited from the KS-DFT calculation. As shown in Table S8 in the SI, the deviations of the CLBEs obtained from KS-DFT eigenvalues ( $\text{CLBE}_n = -\epsilon_n^0$ ) generally increase from C1s to F1s for all DFAs. We expect that, e.g., adding correlation contributions to the RS Hamiltonian would also reduce this undesired species dependence.

The motivation of the RS approach is the reduction of the starting point dependence. As evident from Figure 3(e-h), the large overestimation is observed for all DFAs. Based on the MAEs and MEs in Table 1, it can be shown that the starting point dependence is on average  $< 1$  eV for  $\alpha = 0.0 - 0.45$ . As shown in Figure S2 (SI) for a single water molecule,  $\text{ev}GW_0$  seems to reduce the starting point dependence less. For the same  $\alpha$  range, the CLBE changes by  $\approx 2$  eV. The direct comparison with  $G_0W_0$  is difficult because a unique solution is only obtained for  $\alpha > 0.3$ . However, we can study the change of the CLBEs for  $\alpha = 0.3 - 1.0$ , see Figure S2 (SI), which shows that the starting point dependence is 10 eV with  $G_0W_0$  compared to 2.8 eV with  $\text{ev}GW_0$ .

Moving now to the relative CLBEs, we observe that  $\text{ev}GW_0@PBE$ ,  $G_0W_0@PBEh$ ,  $\text{ev}GW@PBE$  and  $G_{\Delta H}W_0@PBE$  yield MAEs of  $\approx 0.2 - 0.3$  eV, and  $G_{\text{RS}}W_{\text{RS}}$  MAEs of  $0.4 - 0.5$  eV, see Table 1. The errors of the relative CLBEs are centered and tightly distributed around zero for  $\text{ev}GW_0@PBE$ ,  $\text{ev}GW@PBE$  and  $G_{\Delta H}W_0@PBE$ . The perturbative schemes  $G_0W_0@PBEh$  and  $G_{\text{RS}}W_{\text{RS}}$  slightly overestimate the relative CLBEs. The latter is evident from the positive MEs and the error distributions in Figure 3(b,e-h), which are not centered at zero, but exhibit a small offset towards positive values. The RS results show a larger spread compared to  $G_0W_0@PBEh$  and the self-consistent schemes. Furthermore, outliers with errors  $> 1$  eV are observed for  $G_0W_0@PBEh$  and in particular for  $G_{\text{RS}}W_{\text{RS}}$ . The largest outliers are primarily O1s excitations, which originate from the underlying DFT calculation, as evident from Table S8 (see SI), which shows the MAEs of the relative CLBEs from the KS-DFT eigenvalues. For all four functionals (PBE, PBE0, B3LYP, PBEh), we



obtained the largest MAE at the KS-DFT level for the O1s excitations. These errors are inherited in the one-shot  $G_0W_0$  and  $G_{\text{RS}}W_{\text{RS}}$  approaches because of their perturbative nature.

The chemical shifts between CLBES of the same atomic type can be smaller than 0.5 eV for second row elements<sup>4</sup> and even as small as 0.1 eV for C1s.<sup>96</sup> Therefore, the errors for absolute CLBES from  $\text{ev}GW$  and  $G_{\text{RS}}W_{\text{RS}}$  are too large to align or resolve experimental XPS spectra, for which reference data are not available. The most promising methods are  $\text{ev}GW_0@PBE$ ,  $G_0W_0@PBEh$  and  $G_{\Delta H}W_0@PBE$ . With MAEs between 0.2 – 0.3 eV for absolute and relative CLBES, the accuracy is well within the chemical resolution required to interpret most XPS data. The disadvantage of the  $G_0W_0@PBEh(\alpha)$  scheme is the need for tuning the  $\alpha$  parameter. In addition, the species dependence of  $\alpha_{\text{opt}}$  cannot be completely removed. Conversely, the accuracy of  $\text{ev}GW_0@PBE$  and  $G_{\Delta H}W_0@PBE$  is species independent. In addition, the already very good agreement of  $\text{ev}GW_0@PBE$  and  $G_{\Delta H}W_0@PBE$  with experiment might further improve with core-rich basis sets, as already mentioned before.

Comparing  $\text{ev}GW_0$ ,  $G_0W_0@PBEh$  and  $G_{\Delta H}W_0$ ,  $\text{ev}GW_0$  is the computationally most expensive approach. In  $\text{ev}GW_0$ , the eigenvalues are iterated in  $G$  (outer loop) and in each step of the outer loop we iterate Equation (1) (the QP equation) not only for the core state of interest, but for all states. Using exact methods such as contour deformation, the self-energy needs to be re-evaluated at each iteration step of the QP equation, which usually converges within 10 steps. This implies that even for small molecules we evaluate the self-energy in the  $\text{ev}GW_0$  procedure several hundred times. The  $G_0W_0@PBEh$  and  $G_{\Delta H}W_0@PBE$  schemes are computationally significantly less expensive. For  $G_0W_0$ , the QP equation is iterated only once for the core state of interest. Given that the QP equation converges within 10 steps, the total number of self-energy evaluations amounts to 10. The computational cost of  $G_{\Delta H}W_0@PBE$  is only marginally larger than for  $G_0W_0$ . The Hedin shift  $\Delta H$  (see Equation (12)) is computed from  $\Sigma_{1s}(\epsilon_{1s}^0)$  once before the iteration of Equation (10). Given that the latter converges also in 10 steps, the self-energy needs to be calculated 11 instead of 10 times.

Table 2: Absolute C1s CLBEs for ethyl trifluoroacetate (ETFA), see Figure 5(a) for the labels. The deviation  $\Delta_{\text{exp}}$  with respect to experiment and the corresponding mean (ME) and mean absolute errors (MAE) are computed with the experimental data by Travnikova *et al.*,<sup>97</sup> where  $\text{Error}_i = \text{CLBE}_i^{\text{theory}} - \text{CLBE}_i^{\text{exp}}$ .

	C1	C2	C3	C4	ME	MAE
experiment (Gelius <i>et al.</i> <sup>98</sup> )	299.45	296.01	293.07	291.20		
experiment (Travnikova <i>et al.</i> <sup>97</sup> )	298.93	295.80	293.19	291.47		
evGW <sub>0</sub> @PBE	-0.70	-0.54	-0.19	-0.12	-0.36	0.36
G <sub>0</sub> W <sub>0</sub> @PBEh( $\alpha = 0.45$ )	0.56	0.54	0.30	0.16	0.39	0.39
G <sub><math>\Delta</math>H</sub> W <sub>0</sub> @PBE	-0.53	-0.44	-0.10	-0.02	-0.27	0.27
evGW@PBE	0.93	1.01	1.35	1.40	1.17	1.17
G <sub>RS</sub> W <sub>RS</sub> @PBE	3.56	3.70	4.13	4.14	3.88	3.88
G <sub>RS</sub> W <sub>RS</sub> @PBE0	4.41	4.53	4.65	4.51	4.52	4.52
G <sub>RS</sub> W <sub>RS</sub> @B3LYP	4.20	4.29	4.33	4.23	4.26	4.26
G <sub>RS</sub> W <sub>RS</sub> @PBEh( $\alpha = 0.45$ )	5.02	5.13	5.02	4.82	5.00	5.00
evGW <sub>0</sub> @PBE <sup>44</sup>	-0.41	-0.18	-0.04	-0.09	-0.18	0.18
$\Delta$ SCAN <sup>18</sup>	-0.15	-0.08	0.05	0.17	0.00	0.11
$\Delta$ CCSD(T) <sup>8</sup>	-0.35	-0.24	-0.31	-0.23	-0.28	0.28

### 4.3 ETFA molecule

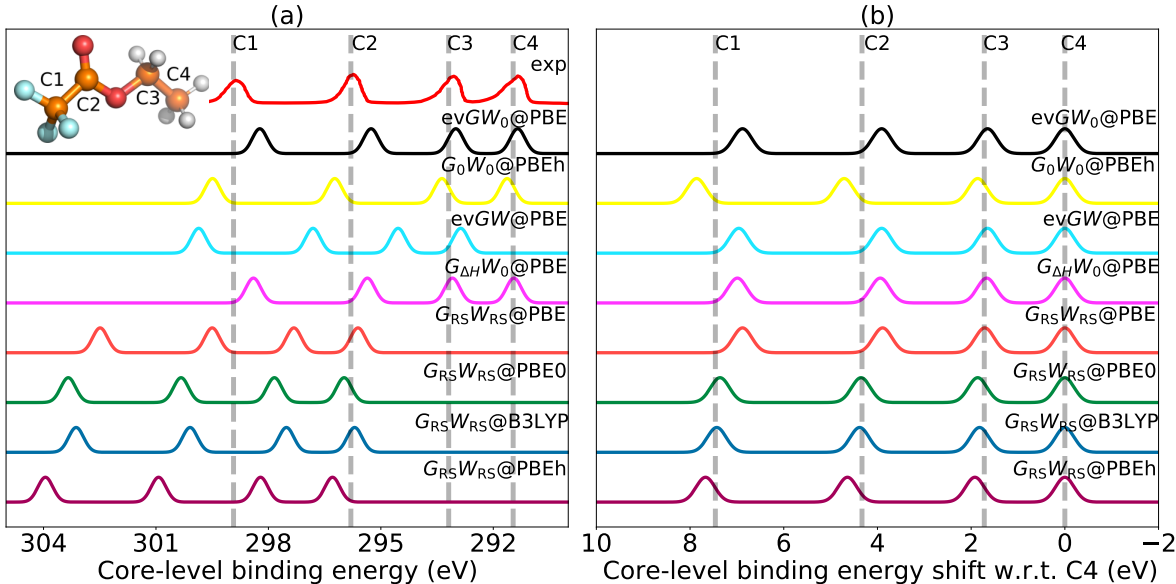


Figure 5: Comparison of the C1s XPS spectrum of ETFA (a) for absolute CLBEs and (b) relative CLBEs obtained from evGW<sub>0</sub>@PBE, G<sub>0</sub>W<sub>0</sub>@PBEh( $\alpha = 0.45$ ), evGW@PBE, G <sub>$\Delta$ H</sub>W<sub>0</sub>@PBE, G<sub>RS</sub>W<sub>RS</sub>@PBE, G<sub>RS</sub>W<sub>RS</sub>@PBE0, G<sub>RS</sub>W<sub>RS</sub>@B3LYP and G<sub>RS</sub>W<sub>RS</sub>@PBEh( $\alpha = 0.45$ ). Dashed lines indicate the experimental reference.

Table 3: Relative C1s CLBEs for ethyl trifluoroacetate (ETFA), see Figure.5 for the labels. The deviation  $\Delta_{\text{exp}}$  with respect to experiment and the corresponding mean (ME) and mean absolute errors (MAE) are computed with the experimental data by Travnikova *et al.*,<sup>97</sup> where  $\Delta_{\text{exp}} = \Delta\text{CLBE}_i^{\text{theory}} - \Delta\text{CLBE}_i^{\text{exp}}$ . The labels of the C atoms are given in the inset of Figure 5(a).

	C1	C2	C3	C4	ME	MAE
experiment (Gelius <i>et al.</i> <sup>98</sup> )	8.25	4.81	1.87	0.00		
experiment (Travnikova <i>et al.</i> <sup>97</sup> )	7.46	4.33	1.72	0.00		
evGW <sub>0</sub> @PBE	-0.58	-0.42	-0.07	0.00	-0.36	0.36
G <sub>0</sub> W <sub>0</sub> @PBEh( $\alpha = 0.45$ )	0.40	0.38	0.14	0.00	0.31	0.31
G <sub><math>\Delta</math>H</sub> W <sub>0</sub> @PBE	-0.50	-0.42	-0.07	0.00	-0.33	0.33
evGW@PBE	-0.47	-0.39	-0.05	0.00	-0.30	0.30
G <sub>RS</sub> W <sub>RS</sub> @PBE	-0.58	-0.44	-0.01	0.00	-0.34	0.34
G <sub>RS</sub> W <sub>RS</sub> @PBE0	-0.10	0.02	0.14	0.00	0.02	0.09
G <sub>RS</sub> W <sub>RS</sub> @B3LYP	-0.03	0.05	0.10	0.00	0.04	0.06
G <sub>RS</sub> W <sub>RS</sub> @PBEh( $\alpha = 0.45$ )	0.21	0.31	0.20	0.00	0.24	0.24
evGW <sub>0</sub> @PBE <sup>44</sup>	-0.32	-0.09	0.05	0.00	-0.12	0.15
$\Delta$ SCAN <sup>18</sup>	-0.32	-0.25	-0.12	0.00	-0.23	0.23
$\Delta$ CCSD(T) <sup>8</sup>	-0.12	-0.01	-0.08	0.00	-0.07	0.07

We further examine the performance of the eight *GW* approaches, which we applied to the CORE65 benchmark set in Section 4.2, for C1s excitations of the ethyl trifluoroacetate (ETFA) molecule, which is also referred to as the ‘ESCA molecule’ in the literature.<sup>97</sup> The ETFA molecule was synthesized to demonstrate the potential of XPS for chemical analysis in the late 1960s. It contains four carbon atoms in various chemical environments, see inset of Figure 5(a). The ETFA molecule presents a challenge because of the extreme variations of the chemical shifts, which range up to 8.0 eV and decrease from the CF<sub>3</sub> to the CH<sub>3</sub> end. The four C1s signals are separated by several electronvolts due to the widely different electronegativities of the substituents on the carbon atoms. ETFA is thus an important reference system and was very recently used to benchmark the performance of different functionals in  $\Delta$ SCF calculations<sup>18,99</sup> and *GW* approaches.<sup>44</sup>

In equilibrium, ETFA exists in two dominating conformations (anti-anti and anti-gauche), i.e., each peak in the spectrum is a superposition of the signals from both conformers.<sup>97</sup> However, including the different conformations is primarily important when resolving the

vibrational profiles of the peaks, which is not the scope of our benchmarking effort. The experimental conformational shifts are  $< 0.1$  eV.<sup>97</sup> To ensure direct comparability with the computational data from Ref. 18, we include thus only the anti-anti conformer.

The first high-quality experimental spectrum of the free ETFA molecule in gas-phase was reported in 1973,<sup>98</sup> while new results were published by Travnikova *et al.* in 2012,<sup>97</sup> see Table 2. Both results were referenced in the most recent studies.<sup>18,44</sup> The newer results have a higher resolution and are vibrationally resolved. More relevant for this work is that the chemical shifts of the more de-screened carbon atoms are significantly larger smaller than in the older spectrum. The difference between the experimental spectra was attributed to missing correction techniques in early multi-channel plate detectors. We follow here the reasoning of Ref. 44, pointing out that coupled-cluster results<sup>8</sup> are significantly closer to the new experimental data (in particular the chemical shifts). We use thus the data by Travnikova *et al.* as experimental reference.

The comparison between the experimental spectrum and calculated spectra are shown in Figure 5. The differences to the experimental peak positions are reported in Table 2 and 3. For the absolute CLBES, the ETFA predictions are inline with the CORE65 benchmark results.  $evGW_0@PBE$  and  $G_{\Delta H}W_0@PBE$  slightly underestimate the CLBES, while  $evGW@PBE$  and the RS schemes severely overestimate them, see Figure 5.  $G_0W_0@PBEh(\alpha = 0.45)$  also overestimates the C1s energies slightly. As discussed in Section 4.2, this is due to the fact that  $\alpha_{opt}$  is slightly smaller than 0.45 for C1s excitation. C1s excitations are consequently slightly overestimated in  $G_0W_0@PBEh$ .  $G_{\Delta H}W_0@PBE$  provides the best accuracy followed by  $evGW_0@PBE$  with an MAE of 0.27 eV and 0.36 eV, respectively, which is consistent with the conclusion for the CORE65 set benchmark.

Turning to the relative CLBES, the three self-consistent schemes and the  $G_0W_0@PBEh$  approach yield MAEs around 0.3 eV, which is only slightly worse than the CORE65 MAEs for C1s.  $evGW_0$ ,  $evGW$  and  $G_{\Delta H}W_0$  underestimate all shifts, while  $G_0W_0@PBEh$  overestimates the shifts of the more "descreened" C atoms (C1 and C2), see Figure 5(b).  $G_{RS}W_{RS}$  also

provides good shifts for ETFA. The RS results are again not completely independent on the starting point. With PBE, the C1s shifts are similarly underestimated as for the self-consistent schemes, while they are slightly too large with PBEh. The RS schemes with the conventional hybrid functionals PBE0 and B3LYP yield, with MAEs below 0.1 eV, the best overall result of the 8 investigated schemes. Furthermore, except for  $G_{\text{RS}}W_{\text{RS}}$  with hybrid starting points, we find that our predictions worsen progressively with the electronegativity of the substituents at the C atoms. The relative CLBEs of C1 ( $\text{CF}_3$ ) and C2 (carbonyl) seem to be the ones that are more difficult to predict, while the predictions of the C3 ( $\text{CH}_2$ ) shifts are mostly within 0.1 eV of the experimental references. However, this trend can be also found in the deviations between the experimental references, see Table 3, i.e., deviations between the experiment values increase with the "descreening" of the C atoms.

Finally, we compare our results to previously published computational XPS data.<sup>8,18,44,97,99-101</sup> We focus here on the results from i) the same method ( $\text{evGW}_0$ ), ii) one of the most successful functionals for  $\Delta\text{SCF}$  ( $\Delta\text{SCAN}$ ) and iii) from a higher-level method (coupled cluster), see Tables 2 and 3. All three literature results include relativistic effects. The previous  $\text{evGW}_0@PBE$  study<sup>44</sup> uses the same correction scheme<sup>49</sup> as employed in this work. The  $\Delta\text{SCAN}$  results were obtained with the atomic zeroth-order regular approximation (ZORA).<sup>78</sup> For the delta coupled cluster doubles results with triples correction ( $\Delta\text{CCSD(T)}$ ),<sup>8</sup> scalar relativistic effects were taken into account by an exact two-component theory. The  $\Delta\text{SCAN}$  and coupled cluster results were computed for the anti-anti conformer, whereas the  $\text{evGW}_0$  literature data are actually an average of the CLBEs of both conformers.

The absolute  $\text{evGW}_0@PBE$  CLBEs from Ref. 44 are less underestimated with respect to experiment in comparison to our results. The largest differences are observed for the descreened C1 and C2 atoms. The previously published  $\text{evGW}_0$  results<sup>44</sup> are not extrapolated, but obtained with a basis sets with more core functions. As already discussed for the CORE65 results, substantially increasing the amount of core functions, seems to cure the (small) systematic underestimation of  $\text{evGW}_0$  for absolute CLBEs. The predictions upon

including more core functions should change on average by 0.25 eV for C atoms,<sup>51</sup> which is close to the (maximal) 0.3 eV difference we observe here. However, similar to our results, the deviation from experiments are larger for C1/C2 than for C3/C4. Since adding the core functions seems to be more relevant for the descreened environments, the chemical shifts improve, too, see Table 3. Some of the difference must be also attributed to the inclusion of the anti-gauche conformer in Ref. 44, which has slightly higher C1s BEs.<sup>97</sup>

We note here that Ref. 44 contains also ETFA results with  $G_0W_0@PBEh(\alpha = 0.45)$  employing core-rich basis sets. However, the  $\alpha$  values was tuned with respect to experiment using an extrapolation scheme with the  $cc\text{-}pVnZ$  basis sets.<sup>48</sup> An insufficiency in the basis set description (i.e. here a systematic underestimation) would be partly absorbed in the  $\alpha$  value, which is the reason why our  $G_0W_0@PBEh$  results will agree better with experiment.

It has been recently shown that the SCAN functional yields excellent absolute and relative CLBEs for molecules<sup>17</sup> and solids.<sup>19</sup> We find that this is also true for the ETFA molecule.  $\Delta$ SCAN yields the best MAE for absolute CLBEs, which is, however, very close to the  $evG_0W_0@PBE$  results<sup>44</sup> with core-function-rich basis set. For the relative CLBEs, the  $\Delta$ SCAN is outperformed by partially self-consistent and RS  $GW$  approaches as well as coupled cluster.

The absolute  $\Delta$ CCSD(T) core excitations<sup>8</sup> are underestimated by 0.23-0.35 eV. However, these results were obtained at the  $cc\text{-}pVTZ$  level and are probably not fully converged.<sup>27</sup> It is thus difficult to judge the performance of the method for absolute CLBEs. The chemical shifts on the contrary are often less affected by the basis set choice and  $\Delta$ CCSD(T) yields together with  $G_{RS}W_{RS}(@PBE0$  or  $@B3LYP)$  MAEs  $< 0.1$  eV.

## 5 Conclusion

We have presented a benchmark study of different  $GW$  approaches for the prediction of absolute and relative CLBEs. In addition to the  $evG_0W_0@PBE$  and  $G_0W_0@PBEh(\alpha = 0.45)$  methods, which were already investigated in Ref. 48, we have included  $evGW@PBE$  and

two new methods, namely  $G_{\Delta H}W_0$  and  $G_{RS}W_{RS}$ , in our study.  $G_{\Delta H}W_0$  is an adaption of the "Hedin shift"<sup>72,74</sup> to core levels and can be considered as computationally less expensive approximation to  $evGW_0$ . In the  $G_{RS}W_{RS}$  approach, the RS Green's function is used as a new starting point and, in contrast to our previous work<sup>65</sup>, also used to compute the screened Coulomb interaction. The purpose of introducing the RS scheme is to reduce the dependence on the starting point and the method has thus been tested with four different DFAs (PBE, PBE0, B3LYP and PBEh( $\alpha = 0.45$ )).

By investigating the self-energy matrix elements and spectral functions, we have confirmed that  $evGW_0@PBE$ ,  $G_0W_0@PBEh$ ,  $G_{\Delta H}W_0@PBE$ ,  $G_{RS}W_{RS}@PBE$ ,  $G_{RS}W_{RS}@PBE0$ ,  $G_{RS}W_{RS}@B3LYP$  and  $G_{RS}W_{RS}@PBEh$  yield a unique solution.  $G_0W_0$  schemes starting from a GGA or hybrid DFT calculation with a low amount of exact exchange do not yield a distinct QP solution. A meaningful physical solution can thus not be obtained with standard approaches such as  $G_0W_0@PBE$ ,  $G_0W_0@PBE0$  and  $G_0W_0@B3LYP$  for CLBEs.

We have studied the CORE65 benchmark set and the C1s excitations of the ETFA molecule with all 8 approaches, for which a physically reasonable solution behavior was confirmed. For the CORE65 set,  $evGW_0@PBE$ ,  $G_0W_0@PBEh$  and  $G_{\Delta H}W_0@PBE$  yield with MAEs of 0.30, 0.33 and 0.25 eV, respectively the best results.  $evGW$  and  $G_{RS}W_{RS}$  overestimate the absolute CLBEs by several electronvolts and are thus not suitable for the prediction of the absolute binding energies. Nevertheless, the RS approaches significantly reduces the starting point dependence as intended. The relative CLBEs are reasonably reproduced with all methods, but in particular with the eigenvalue self-consistent schemes and  $G_{\Delta H}W_0@PBE$  (MAEs  $< 0.2$  eV). The methods exhibit a similar performance for the ETFA molecule, except that the RS approaches with standard hybrid functionals yield here the best chemical shifts.

The  $G_0W_0@PBEh(\alpha)$  approach was introduced in our previous work<sup>48</sup> as computationally affordable alternative to  $evGW_0$  that can mimic to some extent the effect of eigenvalue self-consistency in  $G$ . However, the  $\alpha$ -tuning is methodologically unsatisfying and the optimal

$\alpha$  is dependent on the atomic species. We therefore recommend to use the  $G_{\Delta H}W_0@PBE$  approach instead, which is in terms of computational cost comparable to  $G_0W_0$ .

Finally, we found that  $evGW_0@PBE$  and  $G_{\Delta H}W_0@PBE$  systematically underestimate the experiment. Our comparison to the ETFA literature results and very recent work<sup>51</sup> suggest that this slight, but systematic underestimation can be cured by very large, core-rich basis sets, which might improve the agreement with experiment even further. Future work will consider this and focus on the development of compact and computationally efficient NAO basis sets for core-level  $GW$  calculations.

## SUPPORTING INFORMATION

See the Supporting Information for CORE65 benchmark results, solution behavior of  $G_{RS}W_0$ , errors of KS-DFT for predicting absolute CLBES and relative CLBES, starting point dependence on the tuning parameter in PBEh, geometry of ETFA.

## Acknowledgement

J. L. acknowledges the support from the National Institute of General Medical Sciences of the National Institutes of Health under award number R01-GM061870. W.Y. acknowledges the support from the National Science Foundation (grant no. CHE-1900338). D.G. acknowledges the Emmy Noether Programme of the German Research Foundation under project number 453275048 and P. R. the support from the European Union’s Horizon 2020 research and innovation program under Grant Agreement No. 951786 (The NOMAD CoE). Computing time from CSC – IT Center for Science (Finland) is gratefully acknowledged. We also thank Levi Keller for providing preliminary data for the ETFA molecule.



# Data Availability Statement

The data are available in the SI and the input and output files of the FHI-aims calculations are available from the NOMAD data base.<sup>102</sup>

## References

- (1) Bagus, P. S.; Ilton, E. S.; Nelin, C. J. The Interpretation of XPS Spectra: Insights into Materials Properties. *Surf. Sci. Rep.* **2013**, *68*, 273–304.
- (2) Höfft, O.; Bahr, S.; Himmerlich, M.; Krischok, S.; Schaefer, J. A.; Kempter, V. Electronic Structure of the Surface of the Ionic Liquid [EMIM][Tf<sub>2</sub>N] Studied by Metastable Impact Electron Spectroscopy (MIES), UPS, and XPS. *Langmuir* **2006**, *22*, 7120–7123.
- (3) J. Villar-Garcia, I.; F. Smith, E.; W. Taylor, A.; Qiu, F.; J. Lovelock, K. R.; G. Jones, R.; Licence, P. Charging of Ionic Liquid Surfaces under X-ray Irradiation: The Measurement of Absolute Binding Energies by XPS. *Phys. Chem. Chem. Phys.* **2011**, *13*, 2797–2808.
- (4) Siegbahn, K. *ESCA Applied to Free Molecules*; North-Holland Publishing: Amsterdam; London, 1969.
- (5) Barr, T. L. *Modern ESCA: The Principles and Practice of X-Ray Photoelectron Spectroscopy*; CRC Press: Boca Raton, 2020.
- (6) Aarva, A.; Deringer, V. L.; Sainio, S.; Laurila, T.; Caro, M. A. Understanding X-ray Spectroscopy of Carbonaceous Materials by Combining Experiments, Density Functional Theory, and Machine Learning. Part I: Fingerprint Spectra. *Chem. Mater.* **2019**, *31*, 9243–9255.
- (7) Aarva, A.; Deringer, V. L.; Sainio, S.; Laurila, T.; Caro, M. A. Understanding X-ray Spectroscopy of Carbonaceous Materials by Combining Experiments, Density

- Functional Theory, and Machine Learning. Part II: Quantitative Fitting of Spectra. *Chem. Mater.* **2019**, *31*, 9256–9267.
- (8) Zheng, X.; Cheng, L. Performance of Delta-Coupled-Cluster Methods for Calculations of Core-Ionization Energies of First-Row Elements. *J. Chem. Theory Comput.* **2019**, *15*, 4945–4955.
- (9) Sen, S.; Shee, A.; Mukherjee, D. Inclusion of Orbital Relaxation and Correlation through the Unitary Group Adapted Open Shell Coupled Cluster Theory Using Non-Relativistic and Scalar Relativistic Hamiltonians to Study the Core Ionization Potential of Molecules Containing Light to Medium-Heavy Elements. *J. Chem. Phys.* **2018**, *148*, 054107.
- (10) Hohenberg, P.; Kohn, W. Inhomogeneous Electron Gas. *Phys. Rev.* **1964**, *136*, B864–B871.
- (11) Kohn, W.; Sham, L. J. Self-Consistent Equations Including Exchange and Correlation Effects. *Phys. Rev.* **1965**, *140*, A1133–A1138.
- (12) Parr, R. G.; Yang, W. *Density-Functional Theory of Atoms and Molecules*; Oxford University Press, 1989.
- (13) Bagus, P. S. Self-Consistent-Field Wave Functions for Hole States of Some Ne-Like and Ar-Like Ions. *Phys. Rev.* **1965**, *139*, A619–A634.
- (14) Pueyo Bellafont, N.; Bagus, P. S.; Illas, F. Prediction of Core Level Binding Energies in Density Functional Theory: Rigorous Definition of Initial and Final State Contributions and Implications on the Physical Meaning of Kohn-Sham Energies. *J. Chem. Phys.* **2015**, *142*, 214102.

- (15) Pueyo Bellafont, N.; Álvarez Saiz, G.; Viñes, F.; Illas, F. Performance of Minnesota Functionals on Predicting Core-Level Binding Energies of Molecules Containing Main-Group Elements. *Theor Chem Acc* **2016**, *135*, 35.
- (16) Viñes, F.; Sousa, C.; Illas, F. On the Prediction of Core Level Binding Energies in Molecules, Surfaces and Solids. *Phys. Chem. Chem. Phys.* **2018**, *20*, 8403–8410.
- (17) Kahk, J. M.; Lischner, J. Accurate Absolute Core-Electron Binding Energies of Molecules, Solids, and Surfaces from First-Principles Calculations. *Phys. Rev. Mater.* **2019**, *3*, 100801.
- (18) Klein, B. P.; Hall, S. J.; Maurer, R. J. The Nuts and Bolts of Core-Hole Constrained Ab Initio Simulation for K-shell x-Ray Photoemission and Absorption Spectra. *J. Phys.: Condens. Matter* **2021**, *33*, 154005.
- (19) Kahk, J. M.; Michelitsch, G. S.; Maurer, R. J.; Reuter, K.; Lischner, J. Core Electron Binding Energies in Solids from Periodic All-Electron  $\Delta$ -Self-Consistent-Field Calculations. *J. Phys. Chem. Lett.* **2021**, *12*, 9353–9359.
- (20) Pinheiro, M.; Caldas, M. J.; Rinke, P.; Blum, V.; Scheffler, M. Length Dependence of Ionization Potentials of Transacetylenes: Internally Consistent DFT/GW Approach. *Phys. Rev. B* **2015**, *92*, 195134.
- (21) Golze, D.; Wilhelm, J.; van Setten, M. J.; Rinke, P. Core-Level Binding Energies from GW: An Efficient Full-Frequency Approach within a Localized Basis. *J. Chem. Theory Comput.* **2018**, *14*, 4856–4869.
- (22) Michelitsch, G. S.; Reuter, K. Efficient Simulation of Near-Edge x-Ray Absorption Fine Structure (NEXAFS) in Density-Functional Theory: Comparison of Core-Level Constraining Approaches. *J. Chem. Phys.* **2019**, *150*, 074104.

- (23) Golze, D.; Hirvensalo, M.; Hernández-León, P.; Aarva, A.; Etula, J.; Susi, T.; Rinke, P.; Laurila, T.; Caro, M. A. Accurate Computational Prediction of Core-Electron Binding Energies in Carbon-Based Materials: A Machine-Learning Model Combining DFT and GW. *arXiv:2112.06551* **2021**,
- (24) Hall, S. J.; Klein, B. P.; Maurer, R. J. Self-Interaction Error Induces Spurious Charge Transfer Artefacts in Core-Level Simulations of x-Ray Photoemission and Absorption Spectroscopy of Metal-Organic Interfaces. *arXiv:2112.00876* **2021**,
- (25) Liu, J.; Matthews, D.; Coriani, S.; Cheng, L. Benchmark Calculations of K-Edge Ionization Energies for First-Row Elements Using Scalar-Relativistic Core–Valence-Separated Equation-of-Motion Coupled-Cluster Methods. *J. Chem. Theory Comput.* **2019**, *15*, 1642–1651.
- (26) Vidal, M. L.; Pokhilko, P.; Krylov, A. I.; Coriani, S. Equation-of-Motion Coupled-Cluster Theory to Model L-Edge X-ray Absorption and Photoelectron Spectra. *J. Phys. Chem. Lett.* **2020**, *11*, 8314–8321.
- (27) Ambroise, M. A.; Dreuw, A.; Jensen, F. Probing Basis Set Requirements for Calculating Core Ionization and Core Excitation Spectra Using Correlated Wave Function Methods. *J. Chem. Theory Comput.* **2021**, *17*, 2832–2842.
- (28) Vila, F. D.; Kas, J. J.; Rehr, J. J.; Kowalski, K.; Peng, B. Equation-of-Motion Coupled-Cluster Cumulant Green’s Function for Excited States and X-Ray Spectra. *Front. Chem.* **2021**, *9*.
- (29) Martin, R. M.; Reining, L.; Ceperley, D. M. *Interacting Electrons*; Cambridge University Press, 2016.
- (30) Golze, D.; Dvorak, M.; Rinke, P. The GW Compendium: A Practical Guide to Theoretical Photoemission Spectroscopy. *Front. Chem.* **2019**, *7*.

- (31) Reining, L. The GW Approximation: Content, Successes and Limitations. *WIREs Comput. Mol. Sci* **2018**, *8*, e1344.
- (32) Hedin, L. New Method for Calculating the One-Particle Green's Function with Application to the Electron-Gas Problem. *Phys. Rev.* **1965**, *139*, A796–A823.
- (33) Rasmussen, A.; Deilmann, T.; Thygesen, K. S. Towards Fully Automated GW Band Structure Calculations: What We Can Learn from 60.000 Self-Energy Evaluations. *npj Comput Mater* **2021**, *7*, 1–9.
- (34) van Setten, M. J.; Caruso, F.; Sharifzadeh, S.; Ren, X.; Scheffler, M.; Liu, F.; Lischner, J.; Lin, L.; Deslippe, J. R.; Louie, S. G.; Yang, C.; Weigend, F.; Neaton, J. B.; Evers, F.; Rinke, P. GW100: Benchmarking G0W0 for Molecular Systems. *J. Chem. Theory Comput.* **2015**, *11*, 5665–5687.
- (35) Stuke, A.; Kunkel, C.; Golze, D.; Todorović, M.; Margraf, J. T.; Reuter, K.; Rinke, P.; Oberhofer, H. Atomic Structures and Orbital Energies of 61,489 Crystal-Forming Organic Molecules. *Sci Data* **2020**, *7*, 58.
- (36) Bruneval, F.; Dattani, N.; van Setten, M. J. The GW Miracle in Many-Body Perturbation Theory for the Ionization Potential of Molecules. *Front. Chem.* **2021**, *9*.
- (37) Blase, X.; Attaccalite, C.; Olevano, V. First-Principles GW Calculations for Fullerenes, Porphyrins, Phtalocyanine, and Other Molecules of Interest for Organic Photovoltaic Applications. *Phys. Rev. B* **2011**, *83*, 115103.
- (38) Ren, X.; Rinke, P.; Blum, V.; Wieferink, J.; Tkatchenko, A.; Sanfilippo, A.; Reuter, K.; Scheffler, M. Resolution-of-Identity Approach to Hartree–Fock, Hybrid Density Functionals, RPA, MP2 andGWwith Numeric Atom-Centered Orbital Basis Functions. *New J. Phys.* **2012**, *14*, 053020.

- (39) van Setten, M. J.; Weigend, F.; Evers, F. The GW-Method for Quantum Chemistry Applications: Theory and Implementation. *J. Chem. Theory Comput.* **2013**, *9*, 232–246.
- (40) Bruneval, F.; Rangel, T.; Hamed, S. M.; Shao, M.; Yang, C.; Neaton, J. B. Molgw 1: Many-body Perturbation Theory Software for Atoms, Molecules, and Clusters. *Comput. Phys. Commun* **2016**, *208*, 149–161.
- (41) Wilhelm, J.; Del Ben, M.; Hutter, J. GW in the Gaussian and Plane Waves Scheme with Application to Linear Acenes. *J. Chem. Theory Comput.* **2016**, *12*, 3623–3635.
- (42) Förster, A.; Franchini, M.; van Lenthe, E.; Visscher, L. A Quadratic Pair Atomic Resolution of the Identity Based SOS-AO-MP2 Algorithm Using Slater Type Orbitals. *J. Chem. Theory Comput.* **2020**, *16*, 875–891.
- (43) Zhu, T.; Chan, G. K.-L. All-Electron Gaussian-Based G0W0 for Valence and Core Excitation Energies of Periodic Systems. *J. Chem. Theory Comput.* **2021**, *17*, 727–741.
- (44) Mejia-Rodriguez, D.; Kunitsa, A.; Aprà, E.; Govind, N. Scalable Molecular GW Calculations: Valence and Core Spectra. *J. Chem. Theory Comput.* **2021**, *17*, 7504–7517.
- (45) Aoki, T.; Ohno, K. Accurate Quasiparticle Calculation of X-Ray Photoelectron Spectra of Solids. *J. Phys.: Condens. Matter* **2018**, *30*, 21LT01.
- (46) van Setten, M. J.; Costa, R.; Viñes, F.; Illas, F. Assessing GW Approaches for Predicting Core Level Binding Energies. *J. Chem. Theory Comput.* **2018**, *14*, 877–883.
- (47) Voora, V. K.; Galhenage, R.; Hemminger, J. C.; Furche, F. Effective One-Particle Energies from Generalized Kohn–Sham Random Phase Approximation: A Direct Approach for Computing and Analyzing Core Ionization Energies. *J. Chem. Phys.* **2019**, *151*, 134106.

- (48) Golze, D.; Keller, L.; Rinke, P. Accurate Absolute and Relative Core-Level Binding Energies from GW. *J. Phys. Chem. Lett.* **2020**, *11*, 1840–1847.
- (49) Keller, L.; Blum, V.; Rinke, P.; Golze, D. Relativistic Correction Scheme for Core-Level Binding Energies from GW. *J. Chem. Phys.* **2020**, *153*, 114110.
- (50) Duchemin, I.; Blase, X. Robust Analytic-Continuation Approach to Many-Body GW Calculations. *J. Chem. Theory Comput.* **2020**, *16*, 1742–1756.
- (51) Mejia-Rodriguez, D.; Kunitsa, A.; Aprà, E.; Govind, N. On the Basis Set Selection for Molecular Core-Level GW Calculations. *arXiv:2203.10169* **2022**,
- (52) Yao, Y.; Golze, D.; Rinke, P.; Blum, V.; Kanai, Y. All-Electron BSE@GW Method for K-Edge Core Electron Excitation Energies. *J. Chem. Theory Comput.* **2022**,
- (53) Wilhelm, J.; Hutter, J. Periodic GW Calculations in the Gaussian and Plane-Waves Scheme. *Phys. Rev. B* **2017**, *95*, 235123.
- (54) Ren, X.; Merz, F.; Jiang, H.; Yao, Y.; Rampp, M.; Lederer, H.; Blum, V.; Scheffler, M. All-Electron Periodic  $G_0W_0$  Implementation with Numerical Atomic Orbital Basis Functions: Algorithm and Benchmarks. *Phys. Rev. Mater.* **2021**, *5*, 013807.
- (55) Wilhelm, J.; Golze, D.; Talirz, L.; Hutter, J.; Pignedoli, C. A. Toward GW Calculations on Thousands of Atoms. *J. Phys. Chem. Lett.* **2018**, *9*, 306–312.
- (56) Wilhelm, J.; Seewald, P.; Golze, D. Low-Scaling GW with Benchmark Accuracy and Application to Phosphorene Nanosheets. *J. Chem. Theory Comput.* **2021**, *17*, 1662–1677.
- (57) Duchemin, I.; Blase, X. Cubic-Scaling All-Electron GW Calculations with a Separable Density-Fitting Space–Time Approach. *J. Chem. Theory Comput.* **2021**, *17*, 2383–2393.
- (58) Förster, A.; Visscher, L. Low-Order Scaling Quasiparticle Self-Consistent GW for Molecules. *Front. Chem.* **2021**, *9*.

- (59) Schöne, W.-D.; Eguiluz, A. G. Self-Consistent Calculations of Quasiparticle States in Metals and Semiconductors. *Phys. Rev. Lett.* **1998**, *81*, 1662–1665.
- (60) Caruso, F.; Rinke, P.; Ren, X.; Scheffler, M.; Rubio, A. Unified Description of Ground and Excited States of Finite Systems: The Self-Consistent *GW* Approach. *Phys. Rev. B* **2012**, *86*, 081102.
- (61) Caruso, F.; Rinke, P.; Ren, X.; Rubio, A.; Scheffler, M. Self-Consistent *GW*: All-electron Implementation with Localized Basis Functions. *Phys. Rev. B* **2013**, *88*, 075105.
- (62) van Schilfgaarde, M.; Kotani, T.; Faleev, S. Quasiparticle Self-Consistent *GW* Theory. *Phys. Rev. Lett.* **2006**, *96*, 226402.
- (63) Caruso, F.; Dauth, M.; van Setten, M. J.; Rinke, P. Benchmark of *GW* Approaches for the *GW100* Test Set. *J. Chem. Theory Comput.* **2016**, *12*, 5076–5087.
- (64) Grumet, M.; Liu, P.; Kaltak, M.; Klimeš, J.; Kresse, G. Beyond the Quasiparticle Approximation: Fully Self-Consistent *GW* Calculations. *Phys. Rev. B* **2018**, *98*, 155143.
- (65) Jin, Y.; Su, N. Q.; Yang, W. Renormalized Singles Green’s Function for Quasi-Particle Calculations beyond the *G0W0* Approximation. *J. Phys. Chem. Lett.* **2019**, *10*, 447–452.
- (66) Ren, X.; Tkatchenko, A.; Rinke, P.; Scheffler, M. Beyond the Random-Phase Approximation for the Electron Correlation Energy: The Importance of Single Excitations. *Phys. Rev. Lett.* **2011**, *106*, 153003.
- (67) Ren, X.; Rinke, P.; Scuseria, G. E.; Scheffler, M. Renormalized Second-Order Perturbation Theory for the Electron Correlation Energy: Concept, Implementation, and Benchmarks. *Phys. Rev. B* **2013**, *88*, 035120.



- (68) Li, J.; Chen, Z.; Yang, W. Multireference Density Functional Theory for Describing Ground and Excited States with Renormalized Singles. *J. Phys. Chem. Lett.* **2022**, *13*, 894–903.
- (69) Li, J.; Chen, Z.; Yang, W. Renormalized Singles Green’s Function in the T-Matrix Approximation for Accurate Quasiparticle Energy Calculation. *J. Phys. Chem. Lett.* **2021**, *12*, 6203–6210.
- (70) Zhang, D.; Su, N. Q.; Yang, W. Accurate Quasiparticle Spectra from the T-Matrix Self-Energy and the Particle–Particle Random Phase Approximation. *J. Phys. Chem. Lett.* **2017**, *8*, 3223–3227.
- (71) Zhang, D.; Yang, W. Accurate and Efficient Calculation of Excitation Energies with the Active-Space Particle-Particle Random Phase Approximation. *J. Chem. Phys.* **2016**, *145*, 144105.
- (72) Pollehn, T. J.; Schindlmayr, A.; Godby, R. W. Assessment of the *GW* approximation using Hubbard chains. *J. Phys.: Condens. Matter* **1998**, *10*, 1273–1283.
- (73) Govoni, M.; Galli, G. Large Scale *GW* Calculations. *J. Chem. Theory Comput.* **2015**, *11*, 2680–2696.
- (74) Lee, J. D.; Gunnarsson, O.; Hedin, L. Transition from the Adiabatic to the Sudden Limit in Core-Level Photoemission: A Model Study of a Localized System. *Phys. Rev. B* **1999**, *60*, 8034–8049.
- (75) Rinke, P.; Qteish, A.; Neugebauer, J.; Freysoldt, C.; Scheffler, M. Combining *GW* calculations with Exact-Exchange Density-Functional Theory: An Analysis of Valence-Band Photoemission for Compound Semiconductors. *New J. Phys.* **2005**, *7*, 126–126.

- (76) Ren, X.; Rinke, P.; Joas, C.; Scheffler, M. Random-Phase Approximation and Its Applications in Computational Chemistry and Materials Science. *J Mater Sci* **2012**, *47*, 7447–7471.
- (77) Szabo, A.; Ostlund, N. S. *Modern Quantum Chemistry: Introduction to Advanced Electronic Structure Theory*; Courier Corporation, 2012.
- (78) Blum, V.; Gehrke, R.; Hanke, F.; Havu, P.; Havu, V.; Ren, X.; Reuter, K.; Scheffler, M. Ab Initio Molecular Simulations with Numeric Atom-Centered Orbitals. *Comput. Phys. Commun* **2009**, *180*, 2175–2196.
- (79) Havu, V.; Blum, V.; Havu, P.; Scheffler, M. Efficient O(N) Integration for All-Electron Electronic Structure Calculation Using Numeric Basis Functions. *J. Comput. Phys.* **2009**, *228*, 8367–8379.
- (80) See <http://www.qm4d.info> for an in-house program for QM/MM simulations.
- (81) Perdew, J. P.; Burke, K.; Ernzerhof, M. Generalized Gradient Approximation Made Simple. *Phys. Rev. Lett.* **1996**, *77*, 3865–3868.
- (82) Atalla, V.; Yoon, M.; Caruso, F.; Rinke, P.; Scheffler, M. Hybrid Density Functional Theory Meets Quasiparticle Calculations: A Consistent Electronic Structure Approach. *Phys. Rev. B* **2013**, *88*, 165122.
- (83) Adamo, C.; Barone, V. Toward Reliable Density Functional Methods without Adjustable Parameters: The PBE0 Model. *J. Chem. Phys.* **1999**, *110*, 6158–6170.
- (84) Ernzerhof, M.; Scuseria, G. E. Assessment of the Perdew–Burke–Ernzerhof Exchange–Correlation Functional. *J. Chem. Phys.* **1999**, *110*, 5029–5036.
- (85) Becke, A. D. Density-functional Thermochemistry. III. The Role of Exact Exchange. *J. Chem. Phys.* **1993**, *98*, 5648–5652.

- (86) Lee, C.; Yang, W.; Parr, R. G. Development of the Colle-Salvetti Correlation-Energy Formula into a Functional of the Electron Density. *Phys. Rev. B* **1988**, *37*, 785–789.
- (87) Dunning, T. H. Gaussian Basis Sets for Use in Correlated Molecular Calculations. I. The Atoms Boron through Neon and Hydrogen. *J. Chem. Phys.* **1989**, *90*, 1007–1023.
- (88) Wilson, A. K.; van Mourik, T.; Dunning, T. H. Gaussian Basis Sets for Use in Correlated Molecular Calculations. VI. Sextuple Zeta Correlation Consistent Basis Sets for Boron through Neon. *J. Mol. Struct. THEOCHEM* **1996**, *388*, 339–349.
- (89) Vahtras, O.; Almlöf, J.; Feyereisen, M. W. Integral Approximations for LCAO-SCF Calculations. *Chem. Phys. Lett* **1993**, *213*, 514–518.
- (90) Weigend, F.; Köhn, A.; Hättig, C. Efficient Use of the Correlation Consistent Basis Sets in Resolution of the Identity MP2 Calculations. *J. Chem. Phys.* **2002**, *116*, 3175–3183.
- (91) Sankari, R.; Ehara, M.; Nakatsuji, H.; De Fanis, A.; Aksela, H.; Sorensen, S. L.; Piancastelli, M. N.; Kukk, E.; Ueda, K. High Resolution O 1s Photoelectron Shake-up Satellite Spectrum of H<sub>2</sub>O. *Chem. Phys. Lett* **2006**, *422*, 51–57.
- (92) Schirmer, J.; Angonoa, G.; Svensson, S.; Nordfors, D.; Gelius, U. High-Energy Photoelectron C 1s and O 1s Shake-up Spectra of CO. *J. Phys. B: Atom. Mol. Phys.* **1987**, *20*, 6031–6040.
- (93) Shishkin, M.; Kresse, G. Self-Consistent *GW* Calculations for Semiconductors and Insulators. *Phys. Rev. B* **2007**, *75*, 235102.
- (94) Byun, Y.-M.; Ögüt, S. Practical *GW* Scheme for Electronic Structure of 3d-Transition-Metal Monoxide Anions: ScO<sup>-</sup>, TiO<sup>-</sup>, CuO<sup>-</sup>, and ZnO<sup>-</sup>. *J. Chem. Phys.* **2019**, *151*, 134305.

- (95) Marom, N.; Caruso, F.; Ren, X.; Hofmann, O. T.; Körzdörfer, T.; Chelikowsky, J. R.; Rubio, A.; Scheffler, M.; Rinke, P. Benchmark of GW Methods for Azabenzenes. *Phys. Rev. B* **2012**, *86*, 245127.
- (96) Pireaux, J. J.; Svensson, S.; Basilier, E.; Malmqvist, P.-Å.; Gelius, U.; Caudano, R.; Siegbahn, K. Core-Electron Relaxation Energies and Valence-Band Formation of Linear Alkanes Studied in the Gas Phase by Means of Electron Spectroscopy. *Phys. Rev. A* **1976**, *14*, 2133–2145.
- (97) Travnikova, O.; Børve, K. J.; Patanen, M.; Söderström, J.; Miron, C.; Sæthre, L. J.; Mårtensson, N.; Svensson, S. The ESCA Molecule—Historical Remarks and New Results. *J. Electron Spectrosc. Relat. Phenom.* **2012**, *185*, 191–197.
- (98) Gelius, U.; Basilier, E.; Svensson, S.; Bergmark, T.; Siegbahn, K. A High Resolution ESCA Instrument with X-ray Monochromator for Gases and Solids. *J. Electron Spectrosc. Relat. Phenom.* **1973**, *2*, 405–434.
- (99) Delesma, F. A.; Van den Bossche, M.; Grönbeck, H.; Calaminici, P.; Köster, A. M.; Pettersson, L. G. M. A Chemical View on X-ray Photoelectron Spectroscopy: The ESCA Molecule and Surface-to-Bulk XPS Shifts. *ChemPhysChem* **2018**, *19*, 169–174.
- (100) Van den Bossche, M.; Martin, N. M.; Gustafson, J.; Hakanoglu, C.; Weaver, J. F.; Lundgren, E.; Grönbeck, H. Effects of Non-Local Exchange on Core Level Shifts for Gas-Phase and Adsorbed Molecules. *J. Chem. Phys.* **2014**, *141*, 034706.
- (101) Travnikova, O. et al. Energy-Dependent Relative Cross Sections in Carbon 1s Photoionization: Separation of Direct Shake and Inelastic Scattering Effects in Single Molecules. *J. Phys. Chem. A* **2019**, *123*, 7619–7636.
- (102) Golze, D. Dataset in NOMAD repository. 2022; DOI will be added after revision.

# Graphical TOC Entry

